OPTIMIZATION OF A LIVER ORGAN ON CHIP SYSTEM FOR THE INVESTIGATION OF BREAST CANCER CELL INVASION

Thesis Submitted to
the Graduate School of Engineering and Sciences of
İzmir Institute of Technology
in Partial Fulfilment of the Requirements for the Degree of

MASTER OF SCIENCE

in Molecular Biology and Genetics

by
Perge Bilgesu TOSUNOĞLU

July 2023
İZMİR

We approve the thesis of **Perge Bilgesu TOSUNOĞLU**

Examining Committee Members:

Prof. Dr. Özden YALÇIN ÖZUYSAL
Molecular Biology and Genetics, İzmir Institute of Technology

---

Prof. Dr. Devrim PESEN OKVUR
Molecular Biology and Genetics, İzmir Institute of Technology

---

Associate Prof. Dr. Yavuz OKTAY
Basic And Translational Research Program, Izmir Biomedicine and Genome Center

19/July/2023

Prof. Dr. Özden YALÇIN ÖZUYSAL
Supervisor, Molecular Biology and Genetics
İzmir Institute of Technology

Prof. Dr. Özden YALÇIN ÖZUYSAL
Head of the Department of Molecular Biology and Genetics

Prof. Dr. Mehtap EANES
Dean of the Graduate School of Engineering and Sciences

ACKNOWLEDGEMENT

I would like to thank my supervisor Prof. Dr. Özden Yalçın Özuysal for the continuous guidance and support she had given me in terms of academics and motivation throughout my MSc. journey. I had the chance to learn and try new things thanks to my thesis topic and her open-minded persona. I cannot thank her enough for providing me with the opportunity to talk about academic life in a friendly atmosphere, I feel blessed to have her as my supervisor. I would like to thank Prof. Dr. Devrim Pesen Okvur as well for seeing me as an adopted member of her research group and inviting me to countless outings and meetings. Thanks to her I had two supervisors that supported me throughout this journey. Also, I would like to thank Assis. Prof. Yavuz Oktay for his contributions during my thesis defence seminar.

I am especially grateful to my friend and thesis mate Deniz Cemre Turgut. I feel lucky to have her as a friend and a colleague. As her point of view is different from mine, my perspective has expanded both in my personal life and academics, I learned a lot from her. More than anything I would like to thank her for her continuous mental support throughout this intimidating journey. The past 3 years have become colourful and fun thanks to her.

I am also grateful to Assoc. Prof. Dr. Gülistan Meşe Özçivici and Prof. Dr. Engin Özçivici for their valuable contributions during lab meetings and to my research group members Hülya Doğan, Eda Efe and Z. Elif Günyüz. I would like to thank Dr. Aslı Kısım for making time for me and being a mentor whom I can consult about anything. I am grateful to Dr. Kübra Telli for always supporting me and being a researcher whom I could consult for my worries, as well as for being a friend to me. Lastly, I would like to thank Ata Merdan who helped us in many areas such as chip fabrication and cell culture maintenance. Finally, I would like to thank Prof. Dr. Volkan Seyrantepe and Dr. Seçil Akyıldız Demir for providing the mouse cadavers and making this research possible.

My biggest thanks go to my family and friends, especially my mom who was patient and always listened to me despite all the details and gave me support and ideas even though she had no training on the subject. I appreciate the support of my friends Nehir Yüksel, Zineb Hayatou and N. Ilgım Çelik who were always ready to listen to my troubles and support me in every way possible. Thanks to them I had a place to pour my heart out.

ABSTRACT

OPTIMIZATION OF A LIVER ORGAN ON CHIP SYSTEM FOR THE INVESTIGATION OF BREAST CANCER CELL INVASION

There are many challenges in creating an accurate and physiologically relevant three-dimensional (3D) model of the liver such as finding the suitable liver extracellular matrix (ECM) components and cell types for the development of cell-laden liver-on-a-chip systems. In recent years, precision tissue slice-based methods are used to reduce the problems caused by the cell-laden liver-on-a-chip system complexity. However, these methods require sophisticated tools which are not easily accessible.

This study focuses on the development of a 3D liver model using simple and cost-effective methods. To achieve this, we aimed to optimize liver tissue size, maintenance and culture medium, scaffold gel, and viability assay. The needle method was found to be the easiest, most efficient, and cheap method for tissue processing as the equipment used was easily accessible and evaded enzymatic steps. Moreover, consistent samples that were all similar and in the desired size were easy to obtain. In addition to these, functionality and viability were analysed for 72 hours to assess the physiological state of the liver after tissue processing.

Based on these findings a novel liver-on-a-chip system was successfully developed and as the next step, the invasion of the MDA-MB-231 breast cancer cell line towards the liver was investigated with and without the presence of C-X-C chemokine receptor type 4 (CXCR4) antagonists AMD3100 and AMD3465.

In conclusion, this study demonstrated the development of a novel 3D model for the liver and provided a platform for studying breast cancer invasion with its potential implications for cancer therapy research.

ÖZET

MEME KANSERİ HÜCRELERİNİN İNVAZYON ARAŞTIRMALARI İÇİN BİR KARACİĞER ORGAN ÇİPİNİN OPTİMİZASYONU

Karaciğer fizyolojisini yansıtan bir 3B hücre yüklü yonga-üzeri-karaciğer sistemlerinin geliştirilmesinde, uygun karaciğer hücre dışı matris (ECM) bileşenlerinin ve hücre tiplerinin belirlenmesi gibi zorluklarla karşılaşılmaktadır. Son yıllarda, bu soruna yönelik çözüm olarak doku dilimi tabanlı yöntemler kullanılmaktadır. Ancak bu yöntemler, kolayca erişilemeyen karmaşık ve ileri teknoloji cihazlar gerektirmektedir.

Bu çalışma, basit ve uygun maliyetli yöntemler kullanarak 3B karaciğer modeli geliştirmesine odaklanmaktadır. Bunu başarmak için karaciğer dokusu boyutunun, bakım ve kültür ortamının, jel ortamının ve canlılık testinin optimize edilmesi amaçlanmıştır. Kullanılan ekipmanın kolay erişilebilir olması ve enzimatik basamaklara gerek kalmaması nedeniyle iğne yönteminin en kolay, verimli ve ucuz yöntem olduğu ortaya konmuştur. Ayrıca, bu yöntem ile hepsi birbirine benzeyen ve istenen boyutta tutarlı örnekler elde edilmesi mümkün olmuştur. Bunlara ek olarak, doku işleme adımlarından sonra karaciğerin fizyolojik durumunu değerlendirmek için 72 saat boyunca işlevsellik ve canlılık kontrol edilmiştir.

Bu bulgulara dayanarak, yeni bir yonga-üzeri-karaciğer sistemi başarılı bir şekilde geliştirilmiştir. Ardından, geliştirilen sistem kullanılarak MDA-MB-231 meme kanseri hücre hattının karaciğere doğru invazyonu, C-X-C kemokin reseptörü tip 4 (CXCR4) antagonistleri AMD3100 ve AMD3465 varlığında ve yokluğunda analiz edilmiştir.

Sonuç olarak, bu çalışma ile yeni bir 3B karaciğer modeli optimize edilerek kanser tedavisi araştırmalarında kullanılmak üzere meme kanseri invazyonunun incelenebileceği bir platform geliştirilmiştir.

To all the cancer patients and researchers…

TABLE OF CONTENTS

LIST OF FIGURES

Figure **Page**

LIST OF TABLES

Table **Page**

CHAPTER 1

INTRODUCTION

1.1. Breast Cancer

Cancer is a complex and heterogenous disease described by the spontaneous growth and spread of malignant cells with genetic or epigenetic abnormalities. One of the most malignant and prevalent cancers in women is known to be breast cancer. An analysis of the global cancer statistics revealed that in 2020, breast cancer surpassed lung cancer as the malignancy with the greatest number of 2.3 million new cases. GLOBOCAN (Global Cancer Observatory) data for both sexes showed that breast cancer is the most commonly diagnosed cancer type which covers up to 11.7% of total cases and it is ranked in the top five in terms of mortality. Meanwhile, for women, breast cancer incidence and mortality rank first accounting for 24.5% and 15.5% respectively of all cancer types (Cao et al., 2021; Sung et al., 2021).

Breast carcinoma, which is an epithelial cell-originated malignancy, can be divided into two main types: ductal and lobular carcinoma. Based on where the tumour formed, invasive carcinoma and carcinoma in situ are categorized as ductal and lobular. Epithelial cells proliferate within the duct or lobule in a non-invasive, likely cancerous condition known as ductal or lobular carcinoma in situ (DCIS or LCIS, respectively). On the other hand, carcinoma that has invaded through the basement membrane and infiltrated the stroma and is abnormally proliferating in the breast tissue is referred to as invasive or infiltrative ductal or lobular carcinoma (IDC or ILC, respectively) (Makki, 2015).

Breast cancer can be divided into four main subtypes depending on the presence of receptors. These receptors include the oestrogen receptor (ER), progesterone receptor (PR), and human epidermal growth factor receptor 2 (HER2). The four subtypes are Luminal A (ER^+/PR^+), Luminal B ($ER^+/PR^+/HER2^{-/+}$), HER2 overexpressing ($ER^-/PR^-/HER2^+$), and triple-negative ($ER^-/PR^-/HER2^-$). Triple-negative breast cancers (TNBCs) cannot be effectively treated with hormone therapy or targeted therapy. These TNBCs grow and spread quickly, and have a high risk of metastasis and a bad outlook for

recovery. Patients with TNBCs have a higher chance of relapse and a lower chance of survival than patients without TNBC (Ma et al., 2015; Yeeravalli & Das, 2021).

1.2. Breast Cancer Metastasis to Liver

Metastasis occurs in a multi-step process involving the epithelial-mesenchymal transition (EMT) which generates aggressive cells with stem cell-like properties that degrade extracellular matrix (ECM) (Yeeravalli & Das, 2021). During the spread of cancer, cells move from the original tumour location by invading nearby tissues and entering the bloodstream, then travel throughout the body by surviving in the bloodstream and arresting at distant organs and adjust to survive and grow in new environments by forming small clusters of cancer cells and creating new tumours (Figure 1.1) (Valastyan & Weinberg, 2011).

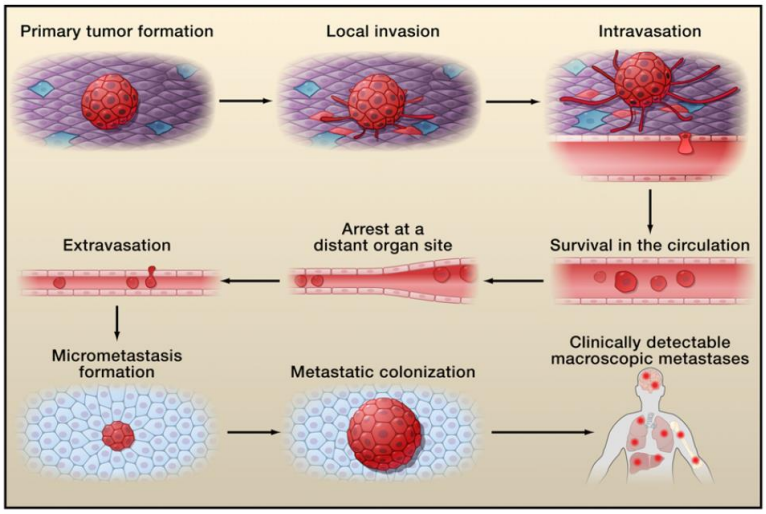

Figure 1.1. Invasion-metastasis cascade scheme. (Source: Valastyan & Weinberg, 2011)

Breast cancer can spread to the bones, lungs, liver, and brain through the bloodstream. When breast cancer spreads to other parts of the body, it often goes to the liver in about 15-32% of cases (Ma et al., 2015; Yeeravalli & Das, 2021). If breast cancer liver metastasis (BCLM) is not treated, the survival time frame is restricted to just 4-8 months.

1.3. CXCL12/CXCR4 Axis in Breast Cancer Metastasis

Chemokines are a group of small secreted peptides that attract cells and control their activities. A C-X-C motif chemokine ligand 12 (CXCL12) also known as stromal-derived-factor-1 (SDF-1) is found in many different types of cells. Acting as a receptor for CXCL12, C-X-C chemokine receptor type 4 (CXCR4) is a rhodopsin-like G protein-coupled cell surface receptor (GPCR) (Yao et al., 2015).

CXCR4 expression is seen in different cancer types including breast cancer and plays a role in the proliferation, chemotaxis, invasion ability, and angiogenesis all of which contribute to the development of tumours and the progression of cancer. The presence of CXCR4 facilitates the breast cancer cell movement out of the bloodstream and then migrates and invades a normal tissue with high amounts of its ligand, CXCL12 (Figure 1.2). The liver is known as one of the sites where CXCL12 is abundantly released which makes it a target for breast cancer metastasis via the CXC12/CXRX4 route (Murphy et al., 2001; Shi et al., 2021).

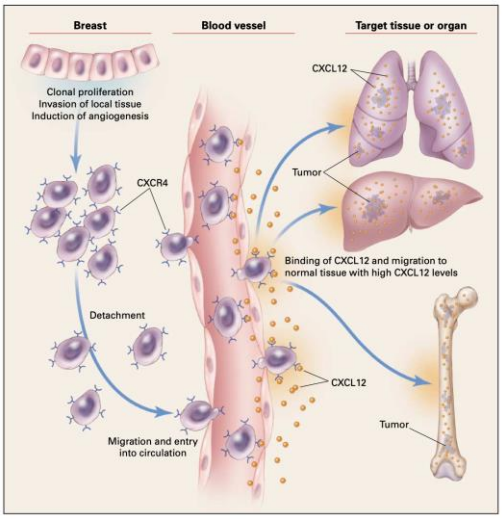

Figure 1.2. CXCR4/CXCL12-mediated breast cancer metastasis. (Source: Murphy et al., 2001)

The most effective antagonists of CXCR4 known at present are a class of drugs referred to as bicyclams (De Clercq, 2015). It has been discovered that a bicyclam called AMD3100 is capable of specifically binding to CXCR4 and blocking the binding

of CXCR4 to CXCL12, thereby impeding the recruitment of macrophages to tumour sites through the disruption of CXCR4/CXCL12 axis (Brenner et al., 2015).

However, AMD3100 is not easily absorbed into the body when taken by mouth because it has a high positive charge. To improve this structural problem an AMD3100 derivative was generated. AMD3465 is a monomacrocyclic second-generation CXCR4 antagonist that lacks these structural limitations (Figure 1.3). AMD3465 is able to keep all the same biological effects as AMD3100 and comparable to AMD3100, hinders the interaction between CXCL12 and cell surfaces. Moreover, studies showed that AMD3465 is demonstrating a slight superiority in inhibiting CXCR4 activity compared to AMD3100 (Hatse et al., 2005; Liu et al., 2021).

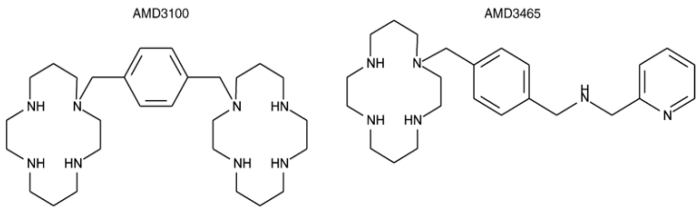

Figure 1.3. Chemical structures of CXCR4 antagonists AMD3100 and AMD3465. (Source: Hatse et al., 2005)

1.4. Cellular and Physiological Properties of Liver

The liver is one of the most complex and heterogenous organs in vertebrates. The hepatic artery and portal vein are two primary blood vessels that are associated with the liver. Oxygenated blood from the aorta is transported by the hepatic artery, while the portal vein carries nutrient-rich blood. These blood vessels divide and form liver sinusoids which are irregularly shaped blood vessels (Schulze et al., 2019).

The cellular architecture of the liver consists of many different cell types (Figure 1.4). The liver is composed of four residing cell types: hepatocytes which are hepatic epithelial cells that makeup 90% of the liver volume, hepatic stellate cells (HSCs) also known as Ito cells are fibrogenic liver cells involved in sinusoidal integrity, Kupffer cells which are known to be liver macrophages and liver sinusoidal endothelial cell (LSECs) that make up the walls of the blood vessels in the liver. In addition to these

cells, there are cholangiocyte cells which are biliary epithelial cells, non-parenchymal cells, and lymphocytes (Schulze et al., 2019; Wernberg et al., 2021).

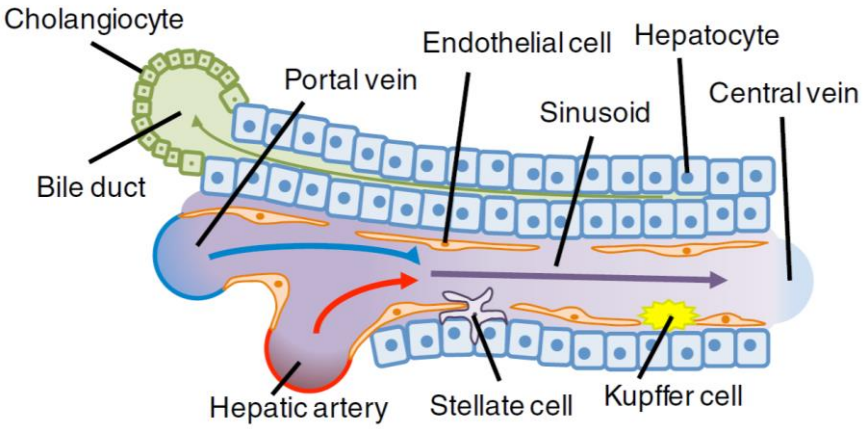

Figure 1.4. Illustration of a sinusoid within the liver. (Source: Trefts, Gannon, & Wasserman, 2017).

Liver ECM is a complex network of proteins that provide support and structure to the liver. It helps in the regulation of various liver functions, including the synthesis and breakdown of substances, as well as the detoxification of harmful substances. The liver ECM also plays a role in the immune response and wound healing of the liver. In normal situations, the liver ECM is made up of collagens (type I, III, IV, V and VI), elastins, proteoglycans, entactin, glycosaminoglycans and glycoproteins like fibronectin and laminin. While the net structure of the liver ECM is formed by collagen type IV, fibril formations are formed by collagen type I, III, V and VI. When there is damage in the liver, HSCs are responsible for extracellular matrix synthesis mainly collagen type I and III (Ye et al., 2020).

Liver damage can be detected by several biochemical markers that are directly related to liver functionality. Hepatocellular injury can be checked via aspartate or alanine aminotransferase (AST and ALT) and alkaline phosphatase (ALP) which are highly concentrated enzymes in healthy liver (Sulava et al., 2017). Additionally, hepatocyte function can also be evaluated by the expression or concentration levels of albumin, a protein synthesized in the liver by hepatic parenchymal cells (Spennati et al., 2021).

1.5. 3D Modelling of Liver

Mimicking the complex *in vivo* hepatic microenvironment in a 3D culture remains a challenge. There are many different liver tissue culture and engineering platforms and nowadays, commonly used 3D liver mimic systems are mainly divided into two categories: cell-laden liver-on-a-chip systems and precision tissue slice (PTS) culture (Moradi et al., 2020).

Chip manufacturing is a preferred method to increase *in vivo* recapitulation. However, the main purpose of these models is to imitate the basic units of tissue, not to create or mimic an entire liver tissue. In cell-laden liver-on-a-chips, one of the hardships is to preserve the cell diversity and ratio of the natural liver. Precisely replicating the liver in a laboratory environment is crucial due to its intricate nature. It is important to select and organize the cells correctly. A cocktail of liver cell types is required to mimic the native liver microenvironment. Commonly, this cocktail consists of hepatocytes, non-parenchymal cells, endothelial cells like HUVEC and EA.hy926 or endothelial-like barriers constructed within the microfluidic system. For hepatocytes, commonly used human cell lines are L-02, HepG2 and C3A or sometimes primary hepatocytes from human or animal models are used (Jia et al., 2020; Kong et al., 2016; Wheeler et al., 2014). In some cases, the differentiation of induced pluripotent stem cells (iPSCs) or hepatic liver stem cells (HLSCs) to hepatocytes is preferred to achieve an unlimited source (Si-Tayeb et al., 2010). In addition to these cell types, to investigate immunological response or perform toxicology testing, cryopreserved human Kupfer cells and stellate cells are used in the development of liver-on-a-chip systems (Ewart et al., 2022). A major disadvantage of these cell-laden platforms is, some of these cells are cancer cell lines and mostly immortalized which deviates from normal physiology. To complete these cell-laden liver-on-a-chip systems, a scaffold gel for ECM coatings such as collagen, hyaluronic acid, alginate, gelatine, Matrigel or decellularized tissue matrix is required for promoting the cell migration, proliferation, differentiation, and adhesion (Yang et al., 2022).

In recent years, there has been a focus on PTS-based methods to reduce the problems caused by cell-laden liver-on-a-chip system complexity. PTS-based systems depend on the correct processing of a whole liver organ. Precision cut liver slices (PCLS) as an *ex vivo* model are obtained by biopsy punch and vibratome. The thickness

of these slices is commonly between 250µm and 700µm. These PCLSs can be originated from murine or humans depending on the research purpose. PCLS is thought to accurately mimic the *in vivo* environment and has the potential to be beneficial for investigating how cancer cells interact with liver-resident cells in addition to screening anti-cancer treatments. In studies with PCLS, ideal liver tissue culture conditions were versatile with some common points such as the usage of DMEM High Glucose or DMEM/F12 as the culture medium. (Khan et al., 2021; Koch et al., 2014; Rodriguez et al., 2019; Shing et al., 2021; Spennati et al., 2021). Koch et al. found that after 72 hours of tissue culture, liver slices are showing decreased expression levels of ATP and in another study done by Spennati et al., changing the culture medium every 24 hours was stated as a crucial step to maintain the viability of the tissue (Koch et al., 2014; Spennati et al., 2021).

Although there are various types of studies using the PCLS approach such as investigating cholestasis or mimicking alcohol-associated liver diseases, it is still a developing application in the field of cancer research. Recently a research group combined the PTS approach with lab-on-a-chip techniques and since the chip system consisted of many layers and was a platform that had to be manually combined gradually, as it was designed according to the placement of the tissue, it was a time-consuming and labour-intensive technique (Tian et al., 2020).

Overall, although there are various types of liver-on-a-chip systems with different research uses, limitations still exist in the generation of liver microenvironment and lab-on-a-chip platforms, indicating that liver-on-a-chip systems remain an open field of research that requires further development.

CHAPTER 2

AIM OF THE RESEARCH

The emerging role of the development of the complex and heterogenous microenvironment of the liver organ in a 3D platform has been recently emphasized, yet there are still gaps that need to be addressed to create a more accurate and physiologically relevant model that closely represents the native liver. Considering the importance of liver ECM components and cellular architecture it is still a challenge. Most of the studies were mainly focused on the organization of 3D cell-laden platforms with artificial or natural scaffold gels which were named liver-on-a-chip systems. Although liver cell cocktails were made according to the purpose of the studies, most of them did not consider the contribution of other ECM components and cell types present in the liver organ which in these cases was not reflecting the most native state of the liver environment. Additionally, the role of the whole liver microenvironment which is required to understand the *in vivo* behaviours of metastatic breast cancer cells towards the liver was not fully studied.

This thesis aimed to investigate the invasion potential of metastatic breast cancer cell line MDA-MB-231 towards the liver by generating a labour-saving, simple, and physiologically relevant liver-organ-on-chip using the intact mouse tissue and lab-on-a-chip (LOC) platform without the requirement of any sophisticated equipment. Therefore, it was aimed to optimize the most efficient tissue processing protocol as well as to maximize the viability and functionality of the obtained tissue for at least 72 hours to investigate MDA-MB-231 invasion within LOC platforms.

CHAPTER 3

METHODOLOGY

3.1. Cell Culture

MDA-MB-231, a human triple-negative basal type invasive breast cancer cell line was obtained from ATCC (HTB-26). It was cultured in DMEM High Glucose (SLD-526-500, Serox) with Fetal Bovine Serum (FBS, A3840001, Gibco, 10%) and Penicillin/Streptomycin (Pen/Strep, 15140122, Gibco, 1%). MDA-MB-231 cell line was stably labelled with a red fluorescent protein (DsRed) by using retrovirus MSCV as described previously (Fıratlıgil-Yıldırır et al., 2021). Cells were cultured at 37°C in a humidified incubator with 5% CO_2.

3.2. Animals

In this research, wild-type mice with C57BL/6 backgrounds between the ages of 8 to 15 weeks were obtained as cadavers from the Laboratory Animal Production, Care, Application and Research Centre at Izmir Institute of Technology. The sex of the mice used in the experiment was random. In accordance with Turkish Council on Animal Care (TCAC) regulations, all mice have been kept and mated in the animal facility at the Izmir Institute of Technology, which has been approved by the TCAC. The Animal Care and Use Committee at the Izmir Institute of Technology in Turkey approved the care and use of animals in the research.

3.3. Tissue Processing

Mice supplied in cadaver form were dissected in a laminar flow hood at room temperature (RT). The liver organ was excised 10-15 minutes after the death of the mouse and placed on a petri dish filled with cold medium (see medium details in Chapter 3.4.1). Table 3.1. shows the details of the different procedures performed on the liver following the dissection. Tissue processing is categorized into 9 subcategories

based on the methods employed and represented as I-IX. All the enzymatic steps were done at 37°C on a rotator meanwhile mechanical steps were done at RT or on ice which was approximately 0-4°C. Before the enzymatic steps, liver tissue was minced with sterile blades until homogenization.

In Process, I, liver tissue was incubated with Trypsin B and Trypsin C (03-052-1B and 03-053-1B, Sartorius) for 30 minutes and 1 hour, respectively. For Processes II-VII, Collagenase (from *Clostridium histolyticum*, C9407, Sigma-Aldrich) and DNase I from bovine pancreas (DNase, DN25, Sigma-Aldrich) were supplied in powder form and dissolved in DMEM/F12 (SLD-521-500, Serox) and ultra-pure H_2O, respectively. An enzyme cocktail with Collagenase and DNase was prepared freshly for each experiment. The enzyme cocktail incubation period was 2 hours to 3 hours for all the processes except II and VI. In these cases, incubation was done overnight. In Processes VI and VII, Trypsin B incubation was done for 5 minutes following the Collagenase and DNase cocktail incubation of liver tissue. After the enzymatic incubations, neutralization was done by adding DMEM High Glucose (SLD-526-500, Serox) with FBS (A3840001, Gibco, 10%). Then centrifuge was done for 5 minutes at 1000 rpm and the pellet was collected for tissue culture.

Processes VIII and IX were mechanical step-only procedures. In VIII, the liver was pieced with a sterile biopsy punch (15110-10, Ted Pella) that had a 1 mm of inner diameter and then with the help of sterile blades these liver pieces were scaled down to 0.5 mm under the stereo microscope. During this process, tissue was in contact with media to prevent excessive drying and necrosis.

For Process IX, a needle (22G, AD722, Techcon) was inserted into a disposable sterile syringe and used for obtaining pieces from the liver tissue. During this process liver tissue was in a cold medium filled petri dish on an ice tray. First, some liquid was drawn into the syringe, then the needle was entered into the tissue and placed in a separate place. With the help of the liquid inside the syringe, tissue pieces (~0.4 mm) were ejected from the needle. Liver pieces were collected in a fresh media and proceeded with tissue culture steps (Chapter 3.4).

Table 3.1. Summary of the enzymatic and mechanical steps for tissue processing.

Process	Mechanical Step	Enzymatic Step	Working Temperature
I	Blades	Trypsin B + Trypsin C	37°C
II	Blades	0.1 mg/ml Collagenase + 0.1 mg/ml DNase	37°C
III	Blades	0.25 mg/ml Collagenase + 0.1 mg/ml DNase	37°C
IV	Blades	1 mg/ml Collagenase + 0.1 mg/ml DNase	37°C
V	Blades	2 mg/ml Collagenase + 0.1 mg/ml DNase	37°C
VI	Blades	0.1 mg/ml Collagenase + 0.1 mg/ml DNase + Trypsin B	37°C
VII	Blades	2 mg/ml Collagenase + 0.1 mg/ml DNase + Trypsin B	37°C
VIII	Biopsy punch ID*: 1mm + Blades	none	RT
IX	Needle gauge: 22G OD**: 0.7176 mm ID: 0.413 mm	none	On ice

*ID: inner diameter,

**OD: outer diameter

3.4. Tissue Culture

3.4.1. Maintenance and Culture Medium

DMEM/F12 (SLD-521-500, Serox) or DMEM High Glucose (SLD-526-500, Serox) based mediums were prepared for liver tissue maintenance and culture as shown in Table 3.2. Serum and other supplements' information is listed below with each medium's purpose of usage. FBS (A3840001, Gibco), Pen/Strep (15140122, Gibco), Donor Horse Serum (DHS, 04-004-1A, Biological Industries), Insulin (I9278, Sigma),

EGF (E9644, Sigma), Cholera Toxin (C8052, Sigma) and Hydrocortisone (H0888, Sigma) supplements were added to the mediums and filtered with vacuum filtration system that had a 0.22μm pore size (99500, TPP) before usage.

Media C-F were used for the viability and liver-on-a-chip experiments. Media A and B were used in the first mouse tissue trials, but it was switched to DMEM/F12-based mediums based on the different articles in the literature indicating that DMEM/F12 is a suitable medium base for tissue culture (Khan et al., 2021; Rodriguez et al., 2019; Shing et al., 2021; Tian et al., 2020).

Table 3.2. Media cocktails used for liver tissue throughout the research.

Media	Medium Base	Serum	Other Supplements	Usage Purpose
A	DMEM High Glucose	none	1% Pen/Strep	Maintenance and Culture
B	DMEM High Glucose	10% Fetal Bovine Serum	1% Pen/Strep	Culture
C	DMEM/F12	none	1% Pen/Strep	Maintenance and Culture
D	DMEM/F12	5% Donor Horse Serum	1% Pen/Strep	Culture
E	DMEM/F12	none	10 μg/mL Insulin 20 ng/mL EGF 1% Pen/Strep	Culture
F	DMEM/F12	5% Donor Horse Serum	10 μg/mL Insulin 20 ng/mL EGF 100 ng/mL Cholera Toxin 0.5 μg/mL Hydrocortisone 1% Pen/Strep	Maintenance and Culture

Liver pieces were incubated at 37°C for 3 hours in Media C or F to remove cell debris and restore ATP content (Spennati et al., 2021) before proceeding with the

culture of pieces in a 96-well plate or embedding them in a scaffold gel for invasion or viability assays (Chapter 3.5.2 and 3.6). After 3 hours of incubation, the media was changed with fresh Media C or F to wash away the cell debris and improve the liver tissue condition. Afterwards, liver pieces were stored at RT until the scaffold embedding and invasion assay development (Chapter 3.6) or tissue viability and functionality assay (Chapter 3.5) setups.

3.4.2. Scaffold Gel

Growth Factor Reduced (GFR) Matrigel (354230, Corning) and Collagen Type I (354249, Corning) were used as scaffold gels for 3D culturing of the liver pieces. Lab-on-a-chip (LOC) platforms which were polydimethylsiloxane (PDMS) based micro-physiological systems were provided by Prof. Dr. Devrim Pesen-Okvur at the Izmir Institute of Technology, Department of Molecular Biology and Genetics. The volume capacity of areas 1 and 3 (A1 and A3) were 40µl and area 2 (A2) had a volume of 20µl (Figure 3.1).

GFR-Matrigel was thawed on ice and then diluted with cold Media C or F in a 1:1 ratio. Then, liver tissue was embedded into the GFR-Matrigel solution with 4.2 mg/ml as the final Matrigel concentration. This mixture was loaded into the A2 of LOCs and polymerization was done at 37°C for 30 min. in humidity.

Collagen type I working solution was prepared for 1.5 and 3 mg/ml as final concentrations according to Table 3.3. First, a 10% HEPES solution was prepared by dissolving powder HEPES (H4034-100G, Sigma) in 10X DMEM High Glucose. Then, the calculated volume of this solution and DMEM/F12, 0.1M NaOH and dH_2O were mixed in an eppendorf tube on ice. Lastly, a Collagen type I stock solution was added to this solution. Similar to Matrigel experiments, liver tissue was embedded into the Collagen type I mixture and polymerization was done at 37°C for 30 minutes in humidity. After polymerization was done for either GFR-Matrigel or Collagen type I, it was proceeded with the invasion assay (Chapter 3.6).

Table 3.3. The required volumes for Collagen type I preparation.

Reagent	Volume
10% HEPES/10X DMEM HG	10 µl
0.1M NaOH	11.5 µl
dH2O	8.5 µl
DMEM/F12	20 µl
Collagen Type I*	50 µl
Total	100 µl

*Stock Conc.: 3 mg/ml or 6 mg/ml

3.5. Tissue Viability and Functionality Assessment

3.5.1. Fluorescent Live/Dead Staining

To determine the viability of the liver pieces, several fluorescent staining dyes and assays were performed on liver tissue as described in Table 3.4. In these assays, Hoechst 33258 (10 mg/ml, 14530-100MG, Sigma), Propidium iodide (PI, 1 mg/ml, P4170, Sigma), Calcein AM (1 mg/ml, C1430, Invitrogen) dyes and Blue/Green Assay Kit (R37609, Invitrogen) were used. After an incubation period at 37°C, Leica SP8 Confocal Microscope was used to measure all samples with excitation and emission wavelengths as described by the manufacturer.

Table 3.4. Summary of fluorescent staining assay protocols.

Assay	Hoechst 33258 / PI	Blue / Green	Calcein AM / PI	Calcein AM / Hoechst 33258
Working Concentrations	**Hoechst 33258:** 33 µg/ml, 1 mg/ml **PI:** 3.3 µg/ml, 2 µg/ml	2 drops of each dye/ml	**Calcein AM:** 2 µg/ml **PI:** 2 µg/ml	**Calcein AM:** 1 µg/ml **Hoechst 33258:** 20 µg/ml
Media	Media F	Media F	Media C, D, E and F	Media C, D, E and F
Assay Platform	96-well plate	96-well plate	96-well plate	96-well plate
Incubation Time	30 min., 1 h, 1.5 h, overnight	15 min., 30 min., 1h	15 min., 30 min., 1h, 2h, overnight	20 min.
Detection Method	Confocal Microscopy	Confocal Microscopy	Confocal Microscopy	Confocal Microscopy

h: hour, min.: minutes

3.5.2. alamarBlue® Assay

To confirm the viability of the liver pieces after the tissue processing steps, another assay, alamarBlue® (873186, Invitrogen), was performed according to the manufacturer's guide. alamarBlue reagent was added in an amount equal to 10% of the culture media volume. Both fluorescent and colourimetric detection were performed.

Liver tissue was embedded in GFR-Matrigel (1:1) into the A2 of LOCs as previously described in Chapter 3.4.2. As an alternative, liver pieces were cultured in a 96-well plate in suspension. Blanks for these setups were liver-free GFR-Matrigel (Matrigel only) and media-only samples, respectively. For negative control, alamarBlue added Matrigel or media were used for LOC and suspension experiments, respectively. Blank samples were done for the spectrophotometer detection method.

Different mediums and platforms were used for alamarBlue. For LOCs, A1 and A3 were used to load alamarBlue added media while for 96-well plate samples were cultured with 80µl media with 10% alamarBlue.

Firstly, to find the optimal incubation time of alamarBlue for the liver tissue, fluorescence intensity was measured in every 4 hours for 24 hours using Leica SP8 Confocal Microscope. After 24 hours imaging was done, media were collected, and colourimetric detection was done by spectrophotometer as well for comparison. This experiment was done by embedding the liver tissue into Matrigel in LOCs and then after polymerization was completed, side areas (A1 and A3) were filled with 10% alamarBlue containing Media F.

After deciding on the optimal incubation time, to understand the effect of Media F on the liver compared to the other DMEM/F12-based mediums (Media C-E, in Table 3.2), liver tissues were incubated with these 4 different mediums. This setup was done for Days 1 and 3, then repeated for Day 3 with the most suitable medium to validate the condition. During these experiments, the effect of 3 hours of incubation at 37°C in Media C and F was also tested. Fluorescence intensity was measured using a Zeiss Axio Observer microscope.

3.5.3. Quantification of alamarBlue® Assay

alamarBlue colourimetric detection quantification was done by following equation 5 of the manufacturer's protocol. Meanwhile, alamarBlue assay quantification for fluorescence intensity was done by collecting the raw images and analysing the fluorescence channel images in ImageJ. Images were stacked and then by the ROI manager an area of 100 by 100 was determined. Mean Gray values of these areas together with the ROI information were saved for each set. The mean Gray value of the sample was divided by the Mean Gray value of the alamarBlue containing Matrigel or media-only samples which were the negative controls of the experiments. Then, descriptive statistics were obtained, and graphs were built by using the mean and standard error values. Lastly, a two-tailed unpaired Student's t-test was performed.

3.5.4. Albumin (BCG) Assay

The functionality of the liver was assessed by using the colourimetric Albumin (BCG) Assay Kit (ab235628, Abcam) by following the manufacturer's protocol. Bromocresol Green (BCG) and albumin interaction results in the emergence of a specific colour detectable at 620nm. For this assay liver pieces were incubated with Media F in a 96-well plate. After plating, every 24 hours for 72 hours media was collected, and an albumin assay was performed (for Days 1, 2, 3). After 20 minutes of incubation at RT, a plate reading was done by spectrophotometer. Albumin concentration calculation was done according to the data sheet and by subtracting the absorbance value of the blank (Media F).

The change in albumin concentration between Day 1 to Day 3 was statistically analysed. First, each sample's reading error was assessed by standard deviation. Then outliers were inspected by applying the z-score test to each day. Afterwards, the mean and standard deviation of the samples for Day 1, Day 2 and Day 3 were calculated, and a bar graph was created. Lastly, a two-tailed unpaired Student's t-test was done to compare three days with each other.

3.6. Invasion Assay

3.6.1. Liver-Organ-On-Chip Development

For the development of liver-organ-on-chip, PDMS-based LOCs provided by Prof. Dr. Devrim Pesen-Okvur at the Izmir Institute of Technology, Department of Molecular Biology and Genetics, were used. Figure 3.1 is a basic illustration of the LOC architecture that was used for invasion assays.

Liver pieces were embedded into either Collagen type I or GFR-Matrigel as described in Chapter 3.4.2, in the A2 of the LOC (Figure 3.1). Then, 40µl of MDA-MB-231-dsRed cells were seeded into one of the A1 of LOCs at the concentration of 1 x 10^6 or 500.000 cells/ml in Media C. Then, 40µl of Media F was loaded into the A3 of the LOCs (Figure 3.1). In the end, LOCs had 20µl of Matrigel or Collagen I (with or without liver) in the A2 and 40µl of cell suspension in A1 and culture media in A3.

The LOCs were then incubated at 37°C for 72 hours. Invasion assay imaging was done using a Leica SP8 Confocal microscope. First images were acquired 2 hours after seeding MDA-MB-231-dsRed cells (Day 0) and then imaging was done every 24 hours for three days (Day 1-3). When a change in the media colour was observed, A3 compartments of the chips were changed with a pre-warmed Media F.

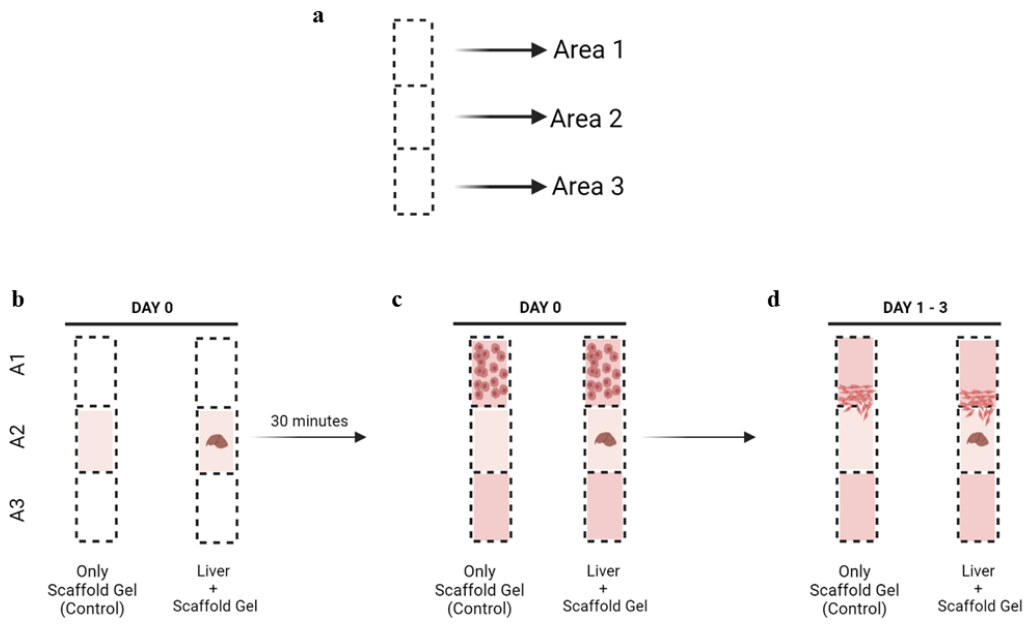

Figure 3.1. Lab-on-a-chip (LOC) platform and invasion assay illustration. Areas of the LOC (a). GFR-Matrigel loading into A2 (b), loading of media and DsRed labelled MDA-MB-231 cells into A1 and media loading into A3 (c). Observation of invading breast cancer cells from A1 to A2 (d). A1: area 1, A2: area 2, A3: area 3.

3.6.2. Drug Treatments on Liver-Organ-On-Chip

To assess the use of the liver-organ-on-chip platform we developed, the effect of two types of CXCR4 antagonists, AMD3100 (A13074, AdooQ Bioscience) and AMD3465 (A11953, AdooQ Bioscience) on MDA MB 231 invasion were analysed. GFR-Matrigel was used as the scaffold gel in the A2. Both drugs were prepared at a final concentration of 20μM or 40μM as these concentrations were found to not affect the viability in 2D culture (data not shown). The four different experimental setups are explained in Table 3.5.

Table 3.5. Summary of invasion assay setups with AMD3100 and AMD3465 drugs.

Set #	Drug Name	Final Concentration	Medium	Drug Loading
1	AMD3100	20μM	Media C	Area 1
1	AMD3465	20μM	Media C	Area 1
2*	AMD3100	20μM	Media F	Area 1
2*	AMD3465	20μM	Media F	Area 1
3	AMD3100	40μM	Media C	Area 1
3	AMD3465	40μM	Media C	Area 1
4**	AMD3100	20μM	Media C Media F	Areas 1, 2 and 3
4**	AMD3465	20μM	Media C Media F	Areas 1, 2 and 3

* In this setup Media F was used for GFR-Matrigel dilution as well, Media F is used in every compartment.

** In this setup Media C was used in A1 and A2 while Media F was used in A3.

The effect of the AMD3100 and AMD3465 on breast cancer metastasis to the liver organ was observed for 72 hours via Leica SP8 Confocal Microscope as previously described. For Set #1 and #2, MDA-MB-231-dsRed cells were prepared with a concentration of 1 x 10^6 cells/ml. Meanwhile, for Set #3 and #4, it was prepared as 500.000 cells/ml.

3.6.3. Quantification of Invasion Assay

Invasion assay quantification was done after collecting the raw images from Day 0 to Day 3. Individual images were obtained for each condition by using the 10X objective of the Leica SP8 Confocal microscope. For each experimental set, the same laser and detector settings were used to prevent bias. Imaging of the LOCs was done by scanning the samples through the scaffold gel margin which was the part between A1 and A2 of the LOCs. Scanning was done with a Z-step size of 7.52µm. For each condition and day interval, the sum projection of z-stacks was constructed (Figure 3.2). The same thresholds are applied to all images. Each bright pixel's distance to the starting line outlining the scaffold gel boundary was calculated using a custom Python program (Ilhan et al., 2020).

The distribution of distances was normalized to Day 0 for each data set and represented by boxplots generated in RStudio. Then two-tailed unpaired Student's t-test was applied to mean values to analyse the significance.

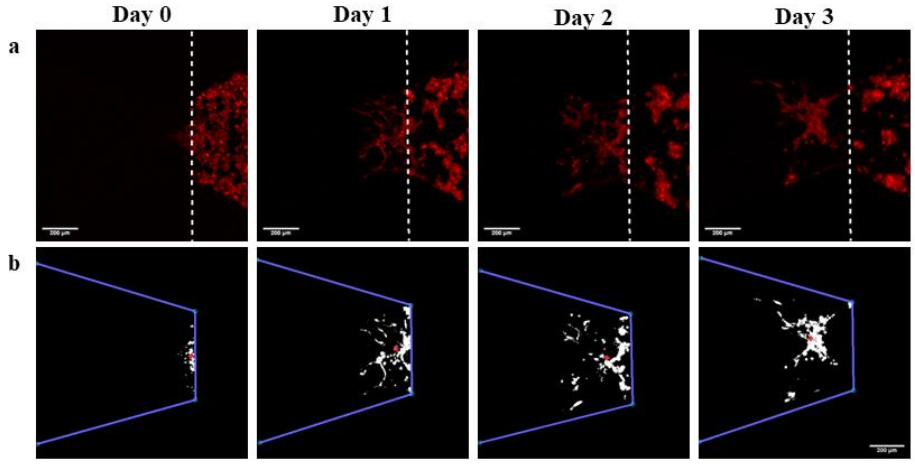

Figure 3.2. A representative figure for LOC invasion analysis. Fluorescence images were obtained with a Z-step size of 7.52µm and collected as a single Z-

stack image by ImageJ for each condition and day (a). Scaffold starting sites (white dotted line) were selected as region of interest (ROI) and the same ROI was applied on different days in ImageJ. By the Python program ROI (b, blue lines) was assigned on the fluorescence images of different days (a). The distance of each bright pixel to the starting line was calculated with Python ("+" specifies the centre of gravity). Scale bar: 200μm.

CHAPTER 4

RESULTS & DISCUSSION

4.1. Liver Tissue Size Optimization

Enzymatic and mechanical processes listed in Table 3.1 were evaluated for time consumption, convenience, and efficiency. In addition to these, the condition of the tissue was assessed by examining any changes in size, integrity, colour, and texture to minimize any potential damage to the tissue.

Size was one of the crucial limitations of our study. The preferred size was between 0.3 to 0.5 mm to facilitate the loading of the tissue containing scaffold gels into the LOC platforms and to ensure an efficient diffusion of media into the tissue. Processes that did not meet this criterion were eliminated and not used in further steps such as alamarBlue, albumin and invasion assays.

For enzymatic processes, it was observed that Collagenase, DNase, Trypsin B and Trypsin C were successful in reducing the size after mincing with blades (Figure 4.1, Process VI and VII). However, the outcome sample was not homogenous in size and there were still cell debris and larger pieces present which resulted in unclear images (Figure 4.1). Performing additional steps like washing with media to reduce the turbidity and heterogeneity of the samples did not improve the result.

Due to the inability to obtain homogeneous and clear samples regardless of the enzyme type, concentration and incubation time, enzymatic procedures were excluded from the subsequent steps.

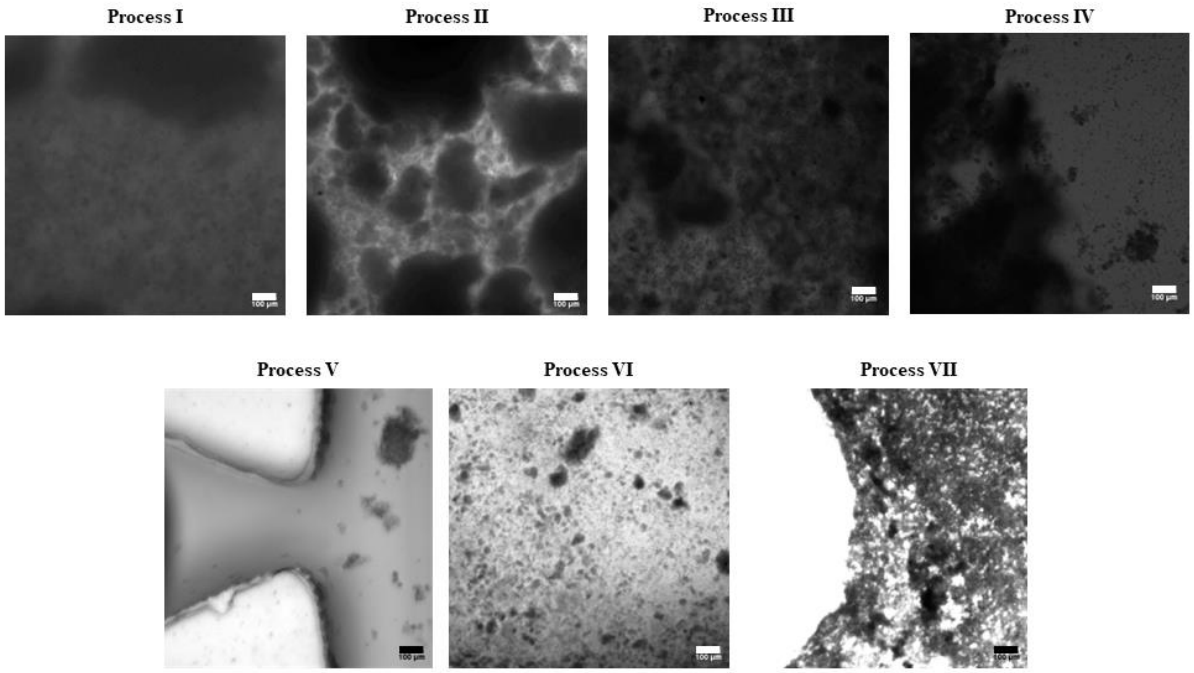

Figure 4.1. Example phase-contrast images of each enzymatic method. Individual images were obtained for each condition by using the 10X objective of the Leica SP8 Confocal microscope. The processed liver tissue was loaded into a LOC platform during Process V. Every other enzymatically processed liver tissue was cultured in a 96-well plate. Scale bar: 100µm.

In Figure 4.2, the used biopsy equipment and application result of Process VIII are shown. With this technique, it was possible to obtain less turbid and more homogeneous samples, but it was a very time-consuming method as the size could not be reduced with a single piece of equipment. In addition to the biopsy punch, sterile blades had to be used to scale down the liver tissue less than a millimetre. Another disadvantage was the working conditions, which were RT and outside the laminar flow hood because of the necessity of stereo microscope usage. The liver is known to be containing various types of enzymes as explained in the introduction and to slow down their effect during tissue processing, it was preferred to work on ice which could not be done on this occasion.

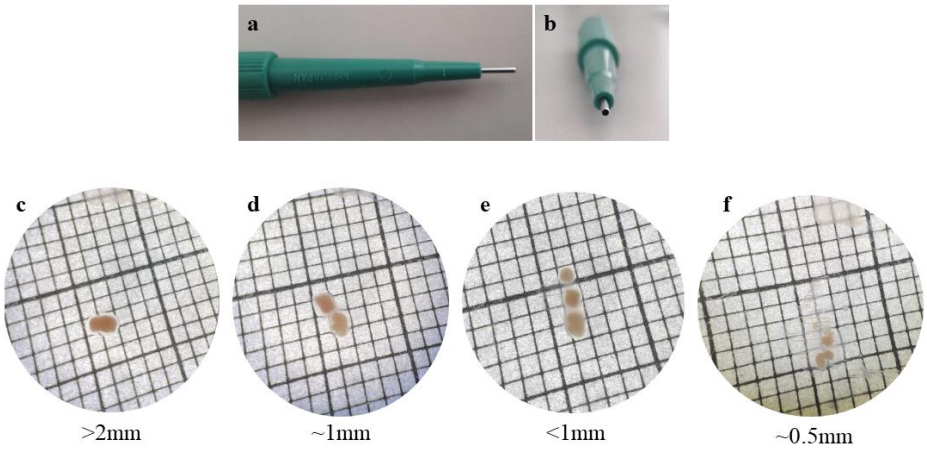

Figure 4.2. Process VIII equipment and application images. A biopsy punch with a 1mm inner diameter (a, b) was used to obtain small pieces from the mouse liver. Pieces were put into a petri dish and under the stereo microscope cut into smaller pieces with the help of a grid paper (c-f). Each side of a small square has a size of 1 mm. The smallest liver tissue size that could be obtained was approximately 0.5 mm.

Considering these factors, a new system was developed that is faster and allows working on ice facilitating the handling of liver tissue. In Figure 4.3, Process IX's workflow is illustrated.

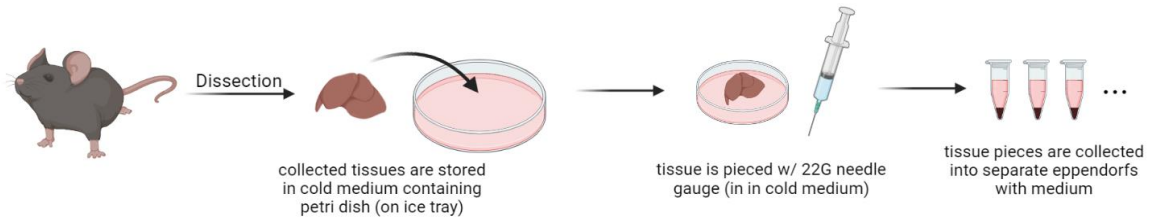

Figure 4.3. Illustration of the workflow of Process IX.

During this process, after mouse dissection and liver organ excision, the working condition was on ice until the liver piece collection and incubation at 37°C. The liver organ was put into a cold medium containing a petri dish on an ice tray and a needle gauge technique was performed. At the end of this process, liver tissue sizes were approximately 0.3 - 0.4 mm and tissue processing was less time-consuming than

Process VIII. As a result of the quick application and cold working environment, tissue integrity was preserved in addition to obtaining pieces of the desired size (Figure 4.4).

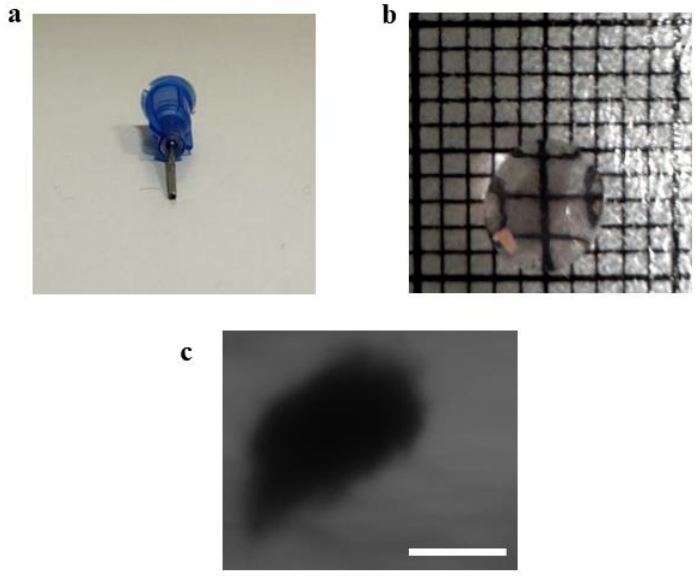

Figure 4.4. Liver tissue after the Process IX application. A needle with a 0.413 mm inner diameter was used to obtain a liver piece (a). Each side of a small square has a size of 1 mm (b). Phase-contrast image of the processed liver piece inside the LOC platform was obtained by using the 10X objective of Leica SP8 Confocal microscope (c). Scale bar: 200μm.

When all the applications in Table 3.1 were compared in terms of advantages and disadvantages, it was decided that Process IX was the most appropriate procedure. Furthermore, out of the nine processes it was the most cost-effective one since no enzymes were used. This protocol, Process IX, was applied for the set-up of liver viability and functionality assessment experiments and invasion assays and will be discussed in the upcoming parts.

4.2. Maintenance and Culture Medium Optimization

4.2.1. Liver Viability Determination

Fluorescent staining assays in Table 3.4 were performed on the liver. Blue-fluorescent dye Hoechst 33258 binds to DNA and as a result stains all the cells (Figure 4.5a and d) meanwhile Calcein AM is a green-fluorescent dye which cannot be retained by apoptotic or dead cells (Figure 4.5c and d). Propidium iodide (PI) is impermeable by live cells and is a red-fluorescent stain that binds to DNA (Figure 4.5a and c). Meanwhile, Blue/Green Assay is a ready-to-use fluorescent viability kit that stains all cells in blue and dead ones in green (Figure 4.5b).

In these setups, liver pieces were cultured in different media as stated in Table 3.4. As shown in Figure 4.5, the fluorescent signal was not specific to cells and a background signal was observed in all samples (Figure 4.5). The reason for a strong background could be poor permeability of the dyes into the liver tissue or non-specific interaction with different tissue components. In conclusion, the effects of media and culture time on viability could not be assessed with the fluorescent live/dead staining assays.

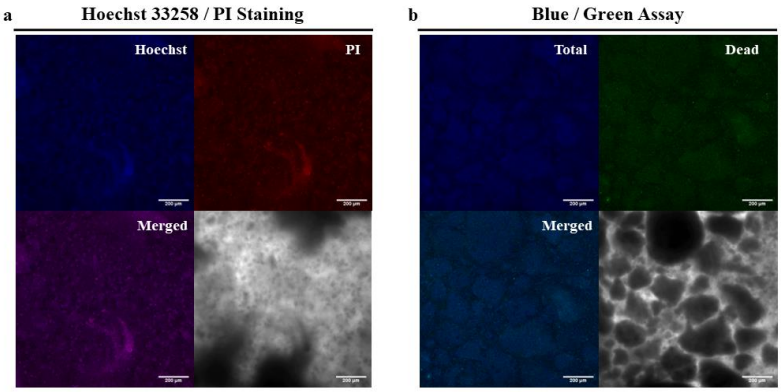

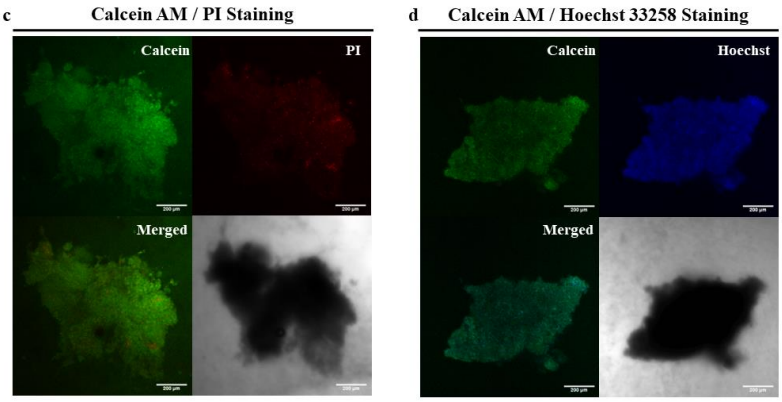

Figure 4.5. Representative samples of each fluorescent live/dead staining assay. The top samples belong to enzymatically processed liver tissue (a, b). Hoechst 33258 /PI staining was performed 72 hours after the tissue was obtained and incubation was done overnight (a). Blue/Green Assay was done on the day the tissue was excised and the sample was incubated for 15 minutes with the dyes. Samples below belong to liver tissues that were processed with Process IX protocol (c, d). Calcein AM/PI staining was performed 24 hours after the tissue was obtained and incubation was done for 20 minutes (c). Lastly, Calcein AM/Hoechst 33258 staining was incubated for 20 minutes and done 24 hours after the tissue was obtained (d). Individual images were obtained for each assay by using the 10X objective of the Leica SP8 Confocal microscope. Scale bar: 200μm.

To overcome the disadvantages of the fluorescent live/dead assays, we switched to the alamarBlue assay. Both colorimetric and fluorescence detection methods were tested for alamarBlue.

The first experimental set-up was done by embedding the liver pieces with Matrigel into LOCs and measuring the fluorescence intensity every 4 hours for 24 hours to find the optimal incubation time for the liver. As shown in the graph (Figure 4.5), from the fourth to twentieth hour, an exponential increase in the values was detected meanwhile there was a decrease between the twentieth hour and the twenty-fourth hour. Prolonged use of alamarBlue can potentially result in diminished functionality of the buffering agents which keep the equilibrium between the oxidized and reduced forms of the indicator. This disrupted equilibrium can cause colour loss which can lessen the detected amount of the reduced form of alamarBlue (O'Brien et al., 2000). Thus, the

data we present was in correlation with a decline in the reduced form of alamarBlue due to prolonged incubation.

As a result of this experiment, 20 hours of incubation of the tissue with 10% alamarBlue at 37°C was selected as the most suitable time compared to other time intervals.

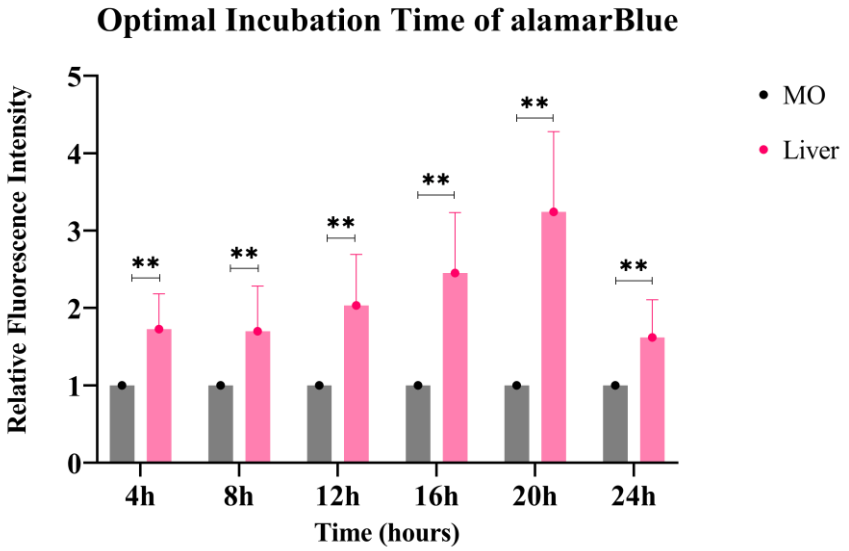

Figure 4.6. The optimal incubation time of alamarBlue for the liver. Liver pieces were obtained from the same mouse and embedded with Matrigel into LOCs. alamarBlue assay was performed 48 hours after liver excision. Matrigel-only samples (MO) were used as blanks. Every 4 hours for 24 hours imaging of the samples was done. Individual images of LOCs were obtained using Leica SP8 Confocal microscope (n=4). ** $p \leq 0.01$

At the end of 24 hours of imaging, media were collected from the LOC channels and colorimetric measurement of alamarBlue was done via spectrophotometry for comparison (Figure 4.7). As seen from the graph, the alamarBlue reduction amount of all liver samples was less than Matrigel-only (MO) control. Colorimetric detection proved to be ineffective for our purpose as the media in the LOC platform and tissue could not be completely extracted for measurement and resulted in inaccurate viability data. Thus, fluorescence intensity measurement was decided to be the most suitable detection method for the viability assessment of the liver.

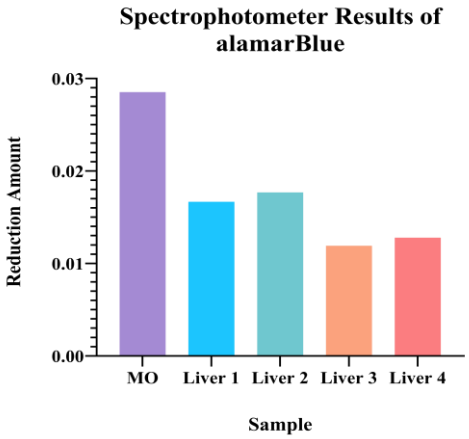

Figure 4.7. Spectrophotometer result of alamarBlue assay for the liver. Liver pieces were obtained from the same mouse and embedded with Matrigel into LOCs. alamarBlue assay was performed 48 hours after liver excision. After fluorescent detection samples were measured with a spectrophotometer. Medium from the Matrigel-only samples (MO) was used as blanks. (n=4).

The next step in the viability assessment was the optimization of culture media. The effect of Media C, D, E and F were tested on liver tissue culture. These media were the candidates as previous studies showed that DMEM/F12 was a suitable medium base for tissue culture (Khan et al., 2021; Rodriguez et al., 2019; Shing et al., 2021; Tian et al., 2020). In this set, liver pieces were embedded with Matrigel into the A2, and candidate mediums were loaded to the A1 and A3. For all the media groups, liver pieces were incubated with Media C at 37°C for 3 hours before embedding into the Matrigel. However, additionally, some samples of the Media F group were incubated at 37°C for 3 hours in Media F to see its effect on the 3 hours of incubation (Figure 4.8, Media F+). This was done depending on a study by Spennati et al., in which they incubated liver sections for 3 hours in media to remove cell debris and restore ATP content (Spennati et al., 2021). alamarBlue assay was performed for Day 1 and Day 3. Figure 4.8 shows the mean values of each media group along with the Matrigel-only (blank) sample. For Day 1, Media C and Media F compared to Media F+ was analysed as not significant however in Day 3 Media F+ showed a significant difference from Media C and Media F. It was observed that using Media F for 3 hours incubation was essential and important to preserve liver viability. Moreover, when compared with MO data, Media

F+ had the highest significance compared to the other groups on Day 3. In accordance with these findings, Media F was chosen both as the maintenance and culture media for the liver.

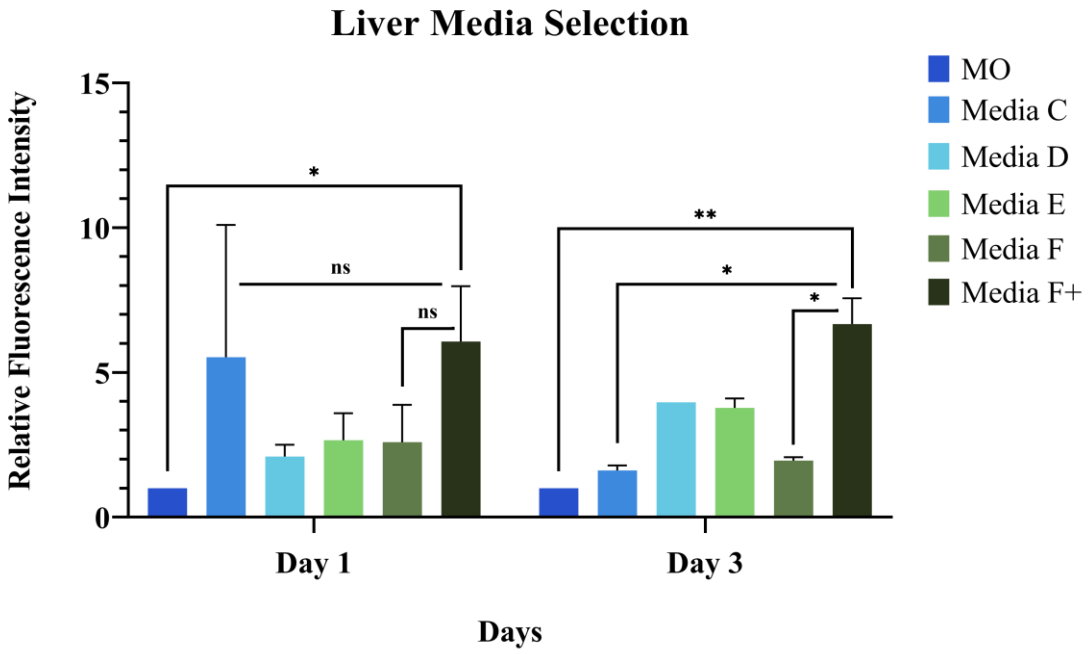

Figure 4.8. Maintenance and culture media selection for the liver. Liver pieces were obtained from the same mouse and embedded with Matrigel into LOCs. Matrigel-only samples (MO) were used as blanks. Imaging of the samples was done after 20-hour incubation. Individual images of LOCs were obtained using a Zeiss microscope (n=3). * $p \leq 0.05$, ** $p \leq 0.01$

The last alamarBlue experiment set was done in order to validate the viability data for Day 3 and to assess whether liver tissue will maintain viability for 72 hours, which is the final time point for the invasion assay (Figure 4.9). For this set, data from 2 different mice were collected. Significant differences between liver and media-only samples were observed thus it was shown that liver samples can survive for up to 72 hours following Process IX.

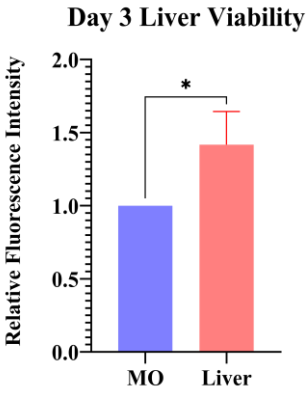

Figure 4.9. Day 3 liver viability. Liver pieces were obtained from the two different mice and cultured with Media F in a 96-well plate. Media-only samples (MO) were used as blanks. Imaging of the samples was done after 20-hour incubation with alamarBlue. Individual images of LOCs were obtained using a Zeiss microscope (n=14). *≤ 0.05

4.2.2. Liver Functionality Assessment

In addition to viability assessment, albumin concentration was analysed to observe whether the liver had maintained functionality. Albumin is a protein synthesized in the liver by hepatic parenchymal cells and its concentration and expression levels are an indicator of liver functionality (Spennati et al., 2021).

48 hours was the minimum required time for the invasion experiments. Hence, an albumin assay was performed every 24 hours for 72 hours to ensure that the tissue does not lose its function in the first 48 hours. Liver pieces were obtained according to the Process IX protocol. Figure 4.10 shows the change in albumin concentration between Day 1 to Day 3 for each sample in detail.

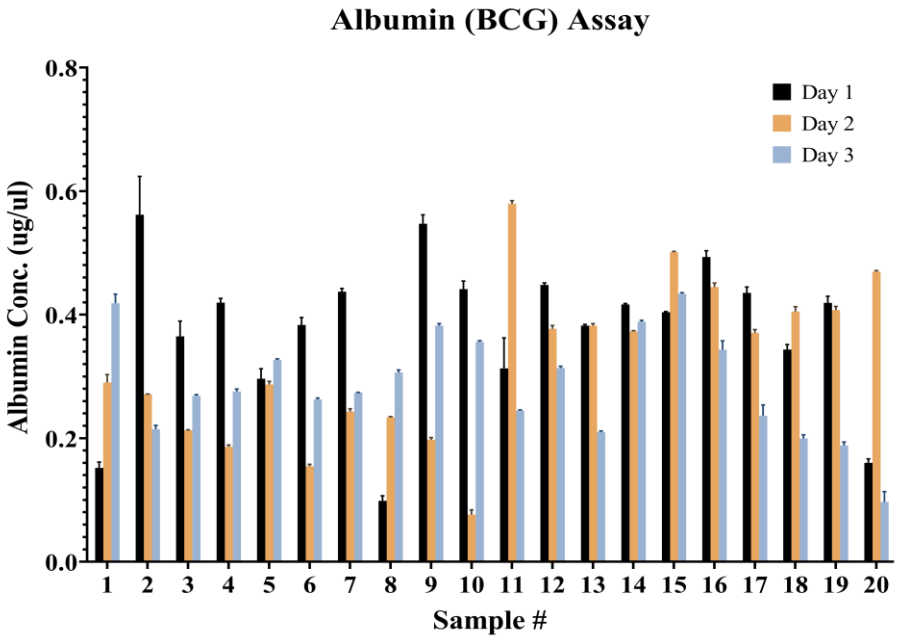

Figure 4.10. Albumin (BCG) Assay graph for each liver sample. Albumin concentration (µg/µl) was detected via spectrophotometer at 620nm. Error bars represent the standard deviation of spectrophotometric readings. The graph reflects the data from 3 independent mouse experiments.

The overall change between each day is shown in Figure 4.11. Albumin concentration differences between Day 1 versus Day 2 and Day 2 versus Day 3 were not significant while in Day 3 albumin concentration significantly decreased compared to Day 1. This was an expected result as 72 hours was stated as the maximum possible culture time for liver tissue in other studies as hepatocytes are known to become necrotic within 72 hours (Koch et al., 2014; Spennati et al., 2021).

However, the overall change in albumin concentration was not drastic which supported the idea that liver pieces had maintained functionality after dissection and mechanical process. This finding confirmed that the established liver-organ-on-chip system is functional and does not cause significant damage to the liver tissue.

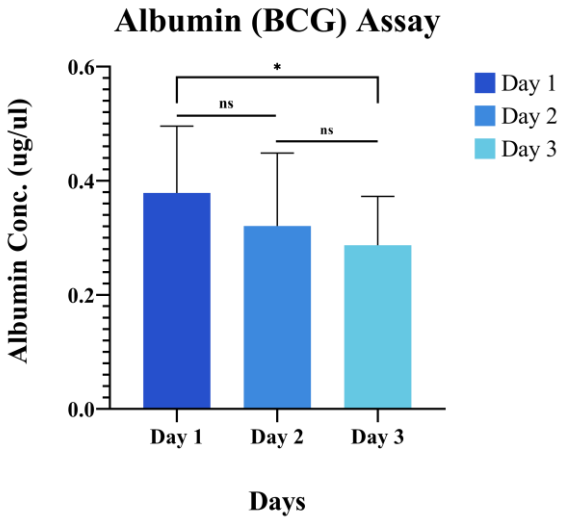

Figure 4.11. Albumin (BCG) Assay graph for each day. The mean and standard deviation of each day was calculated, and Student's t-test was applied to compare each day (n=20). * $p \leq 0.05$

To sum up, viability and functionality assessments showed that liver pieces can preserve their physiology for up to 72 hours which meets the required time frame for the invasion experiments. Moreover, it was determined that Media F was the most suitable culture and maintenance media for the liver. This could be because of the presence of a cortisol mimic hydrocortisone and insulin in Media F, which are known to be stimulating the synthesis of albumin (Spada et al., 2021).

4.3. Optimized Workflow Summary

When the methods with the best efficiency and results were brought together after the tissue processing and media optimizations, a workflow like the one in Figure 4.12 emerged.

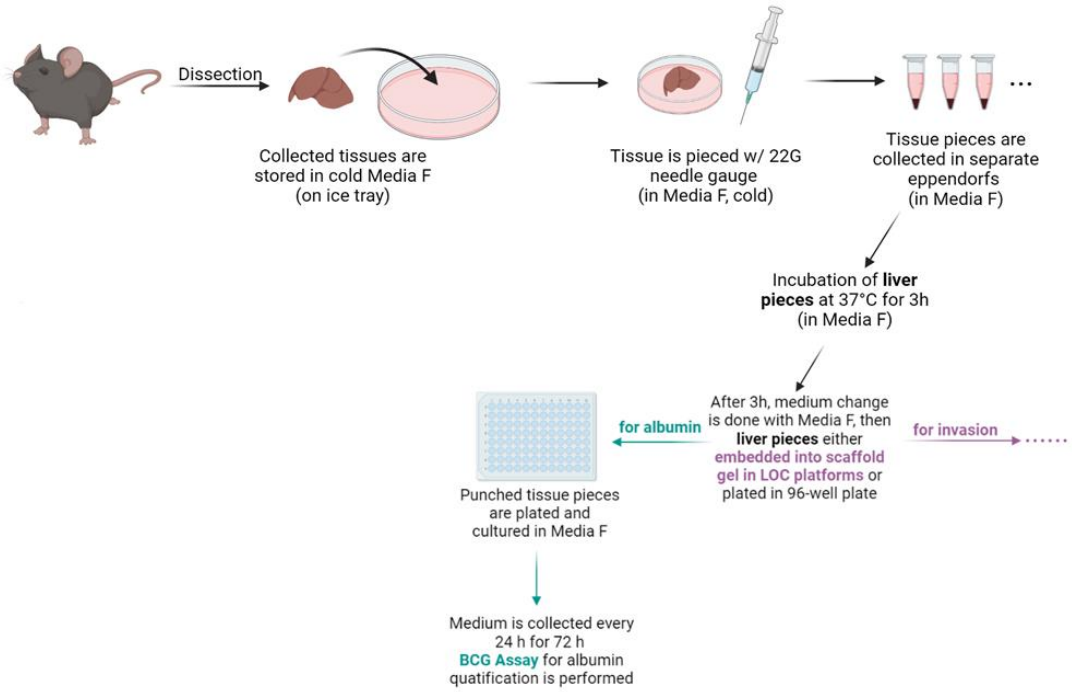

Figure 4.12. Schematic representation of the optimized workflow.

4.4. Invasion Assay

4.4.1. Scaffold Gel Optimization

Collagen type I and GFR-Matrigel were preferred as the scaffold gels in this research. Collagen type I is one of the main components of liver ECM which made it a candidate for 3D matrix modelling in this study. Also, it is a commonly used scaffold component for *in vitro* studies (Khan et al., 2014; Shing et al., 2021).

Meanwhile, GFR-Matrigel is a substance that creates a natural environment for biological processes. It is commonly used in various applications, such as creating 3D environments that mimic native conditions. It is a complex mixture that includes laminin, collagen type IV and proteoglycan which is compatible with the natural microenvironment of the liver (Hughes et al., 2010; Ye et al., 2020). The purpose of utilizing GFR-Matrigel was to counteract the effects of growth factors on breast cancer cells and investigate the effect of the liver microenvironment on invasion.

Control groups of gel optimization were prepared by diluting the gels with media without any liver piece addition. Experiment groups were prepared by embedding one liver piece into the scaffold gel per LOC. Scaffold gels were diluted with Media C for all the setups in this part. Final concentrations for Collagen type I were 1.5 and 3 mg/ml, meanwhile 4.2 mg/ml was used for GFR-Matrigel.

Figure 4.13 shows the Collagen type I experiments. In the case of 1.5 mg/ml, Collagen type I folded right after embedding the liver pieces and continued to deteriorate further until Day 3 (Figure 4.2a). When 3 mg/ml Collagen type I was tested it showed no immediate disruption but at the end of Day 3 the gel folded onto itself and the liver piece (Figure 4.2b). A slight bump which was indicated with a red arrow in Figure 4.13 shows this disruption in the LOC platform.

As a result of these findings, it was decided that Collagen type I is not a suitable scaffold gel for our experiments. The reason behind this gel disruption can be because of the abundant enzyme concentration in the native liver. In other words, secretion of the enzymes following Process IX application could result in the disruption of the collagen gel.

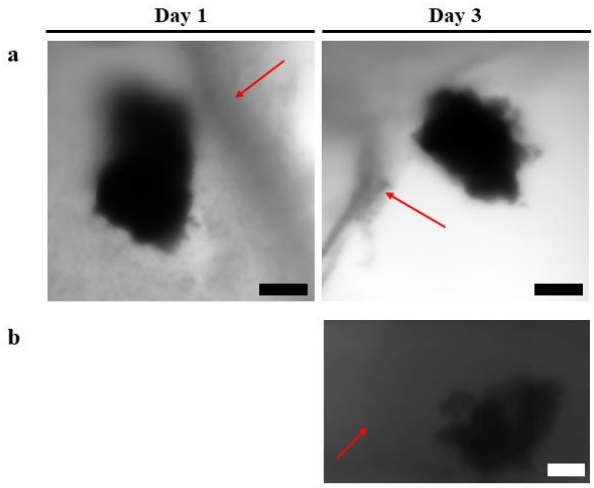

Figure 4.13. Result of Collagen type I usage as the scaffold gel. Representative phase-contrast images of 1.5 mg/ml (a) and 3 mg/ml (b) Collagen type I from Day 1 and Day 3. Individual images were obtained by using the 10X objective of the Leica SP8 Confocal microscope. Red arrowheads show the folding of Collagen type I. Scale bar: 200μm.

Another option for scaffold gel was GFR-Matrigel which was used in a previous study for 3D cell culture applications (Firatligil-Yildirir et al., 2021). Taking this study into account, GFR-Matrigel was used for liver piece embedding with a final concentration of 4.2 mg/ml, there were no visible disruptions (data not shown). Since its content and usage purposes were suitable for our experiments, GFR-Matrigel was decided as the scaffold gel for invasion trials.

4.4.2. Invasion of Metastatic Breast Cancer Cell Line to Liver

The effect of liver presence on MDA-MB-231 invasion was investigated by using GFR-Matrigel-only LOCs as the control group. For the experiment group liver was embedded into GFR-Matrigel in A2 of LOCs. DsRed-labelled MDA-MB-231 cells were loaded into A1 in Media C and for both groups, Media F was loaded into A3 compartments. The invasion was screened from Day 0 to Day 3.

Figure 4.14 shows a significant difference in the distance taken between the control and experimental group (liver). In both conditions, invasion increased from Day 0 to Day 3, which is a compatible finding with the invasive characteristics of MDA-MB-231. However, in the presence of the liver, an increased invasion of MDA-MB-231 cells towards A2 was observed compared to the control group. Accordingly, the liver-organ-on-chip platform was able to show the effect of the liver as a chemoattractant both visually and quantitatively.

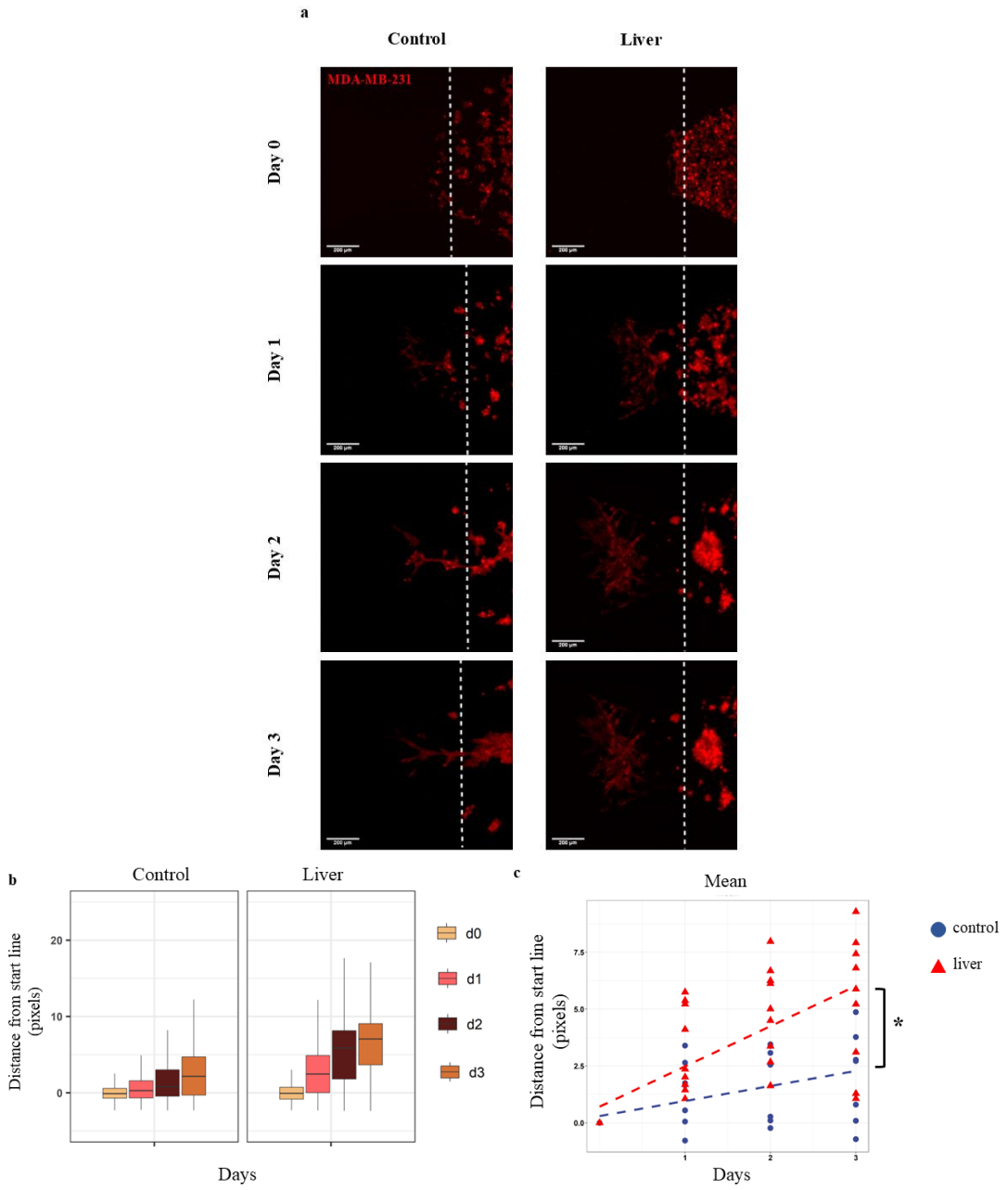

Figure 4.14. Invasion of MDA-MB-231 cells towards control versus liver. Representative Z-stack images of MDA-MB-231 cells (red) invasion towards a) empty (control) or liver-embedded Matrigel (dashed line represent the invasion starting line) (Scale bar: 200µm). b) Each bright pixel's distance to the starting line was calculated after thresholding of Z-stack images. The data normalized to Day 0 were plotted. c) Mean values of normalized distance distributions were plotted for Day 0 to Day 3. Liver pieces were obtained from 4 independent mouse experiments. (n=7, 9). * $p \leq 0.05$

4.4.3. Drug Trials for Invasion Assay

After the demonstration of breast cancer cell invasion towards the liver was successful on the liver-organ-on-chip system we developed, drug trials were conducted. The effects of CXCR4 antagonists AMD3100 and AMD3465 on MDA-MB-231 invasion behaviour were investigated. For this, four different sets of experiments were done (Table 3.5).

The first set was done by loading 4.2 mg/ml into the A2 for the control group and embedding the liver piece into 4.2 mg/ml Matrigel for the experiment group. After Matrigel polymerization, A3 compartments were loaded with Media F for both groups. Then, loading MDA-MB-231-dsRed cell into the A1 with or without 20μM AMD3100 or AMD3465 in Media C was done for both groups.

Figure 4.15 shows the visual and quantitative effect of this first drug trial. At the end of this setup, contradictory findings to the previous experiments (Figure 4.14) were obtained such as the presence of liver did not show any significant difference compared to the Matrigel-only control group. This could be because of the small sample population of the experimental set-up. Meanwhile, AMD3100 and AMD3465 presence did not show any significant inhibition of invasion either in the control or liver group to their drug-free controls. Liver AMD3100 and AMD3465 were compared with the control AMD3100 and AMD3465 and did not show any significance as well. In this case, this result was not expected as AMD3100 and AMD3465 are known to be inhibiting the CXCR4/CXCL12 axis by specifically binding to CXCR4 and blocking the binding of CXCR4 to CXCL12 (Brenner et al., 2015). Moreover, the liver organ is known as one of the sites where CXCL12 is abundantly released (Murphy et al., 2001; Shi et al., 2021), and depending on this information a decrease in MDA-MB-231 invasion in the presence of 20μM AMD3100 or AMD3465 was expected.

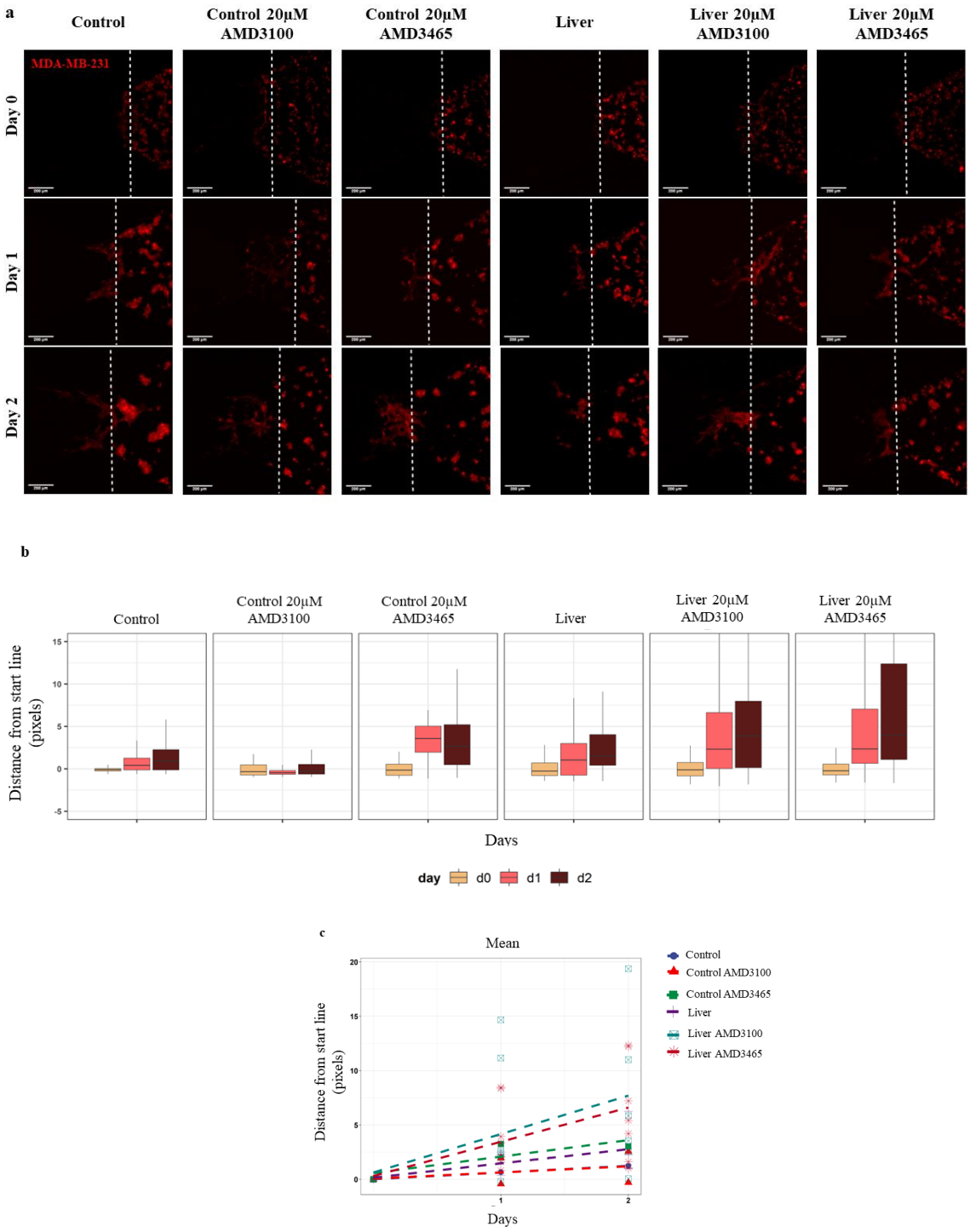

Figure 4.15. Invasion of MDA-MB-231 cells towards control versus liver in 20µM AMD3100 / AMD3465 presence and absence. Representative Z-stack images of MDA-MB-231 cells (red) invasion towards a) empty or liver-embedded Matrigel (dashed line corresponds to the starting line for invasion) with the effect of CXCR4 antagonists (AMD3100 and AMD3465) (Scale bar: 200µm). b) Each bright pixel's distance to the

starting line was calculated after thresholding of Z-stack images. The data normalized to Day 0 were plotted. c) Mean values of normalized distance distributions were plotted for Day 0 to Day 2. All samples were not significant (not shown in the graph). Liver pieces were obtained from 2 independent mouse experiments. (n=2-7).

Taking into account that the use of different media compositions in A1 and A3 might affect the invasion potential, the entire chip system was constructed by using Media F for all the compartments of LOC to preserve a chemical equilibrium. Matrigel was diluted with Media F to obtain a final concentration of 4.2 mg/ml. Then, A3 was loaded with Media F (this one was the usual protocol). Another change was the seeding of MDA-MB-231 cells. Normally Media C was used for A1 however in this set Media F was used to prepare 20μM AMD3100 or AMD3465 and for the drug-free group.

It was observed that rather than preferring to invade towards A2, MDA-MB-231 cells stayed in the A1 which was loaded with Media F (Figure 4.16). Between Day 0 and Day 1, all the samples invaded the Matrigel containing A2. For liver AMD3100 and control AMD3465, cells migrated away from the start point meanwhile other samples showed a decrease between Day 0 and Day 3. However, the differences in the invasion did not reach a statistically significant value (Figure 4.16c). Drug-free control and the liver group's migrating cells were not significantly different which did not match the initial data from the invasion assay experiments (Figure 4.14), it is considered to be the result of the small sample group.

In summary, in this setup, most of the cells preferred to stay in the Media F-containing environment which was a supplement-rich medium. After a while, cells proliferated thanks to the supplements such as EGF, serum and insulin and resulted in a quick media consumption as was observed from the colour change in the A1 compartment and cells started to form clumps starting from Day 1.

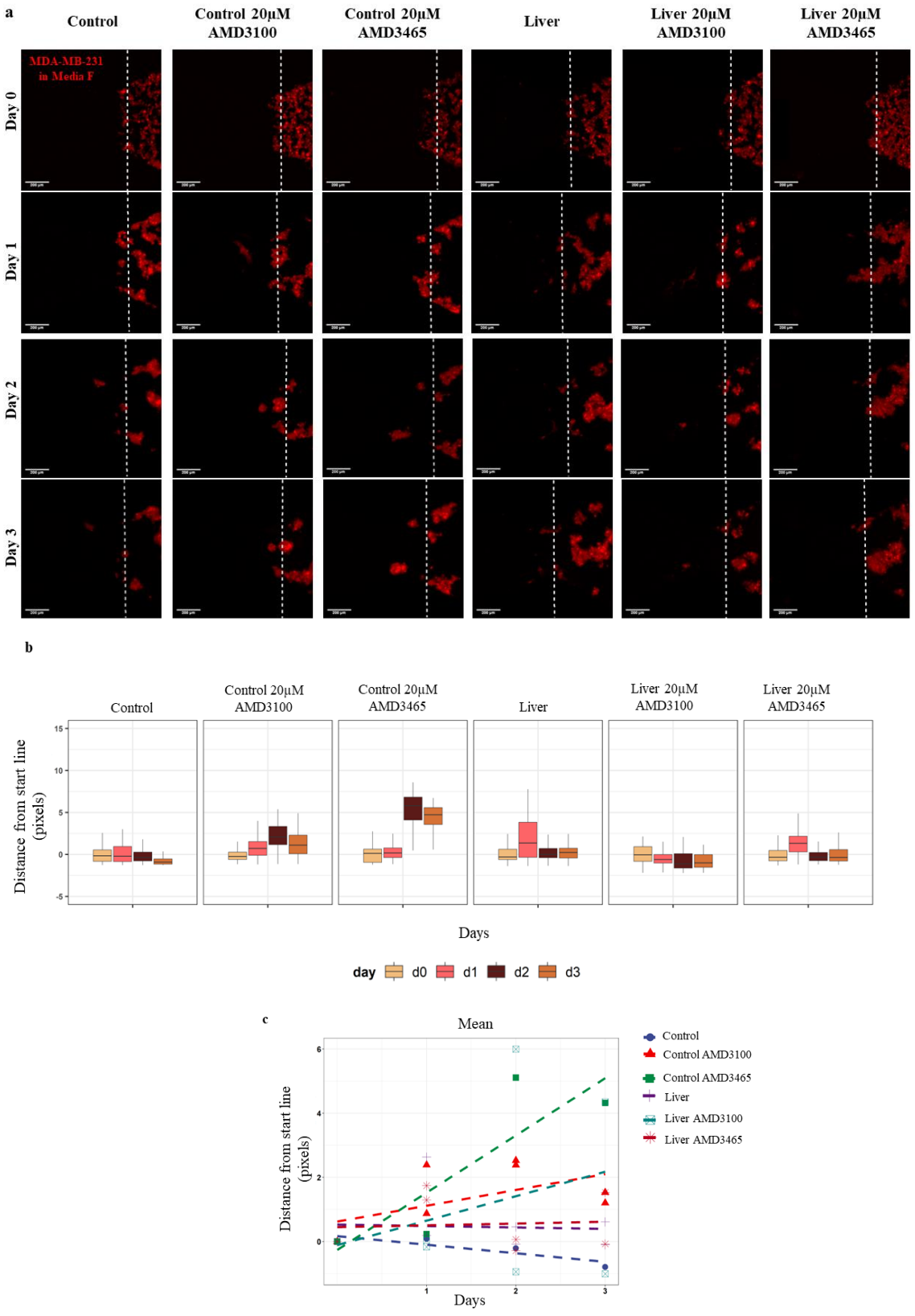

Figure 4.16. Invasion of MDA-MB-231 cells in Media F towards control versus liver in 20µM AMD3100 / AMD3465 presence and absence. Representative Z-stack images of MDA-MB-231 cells (red) invasion towards a) empty

or liver-embedded Matrigel (dashed line corresponds to the starting line for invasion) with the effect of CXCR4 antagonists (AMD3100 and AMD3465) (Scale bar: 200μm). b) Each bright pixel's distance to the starting line was calculated after thresholding of Z-stack images. The data normalized to Day 0 were plotted. c) Mean values of normalized distance distributions were plotted for Day 0 to Day 2. Liver pieces were obtained from the same mouse. All samples were not significant (not shown in the graph). (n=2).

Overall, this data did not reveal the effect of CXCR4 antagonists. Using Media F in A1 was not preferred as the cancer cells chose proliferation over invasion in this setup. In light of these findings, the third and fourth drug trials were done by seeding MDA-MB-231 cells in Media C in A1 of the LOCs.

The third drug experiment set was done similarly to the first drug set with a slight change which was increasing the concentration of AMD3100 and AMD3465. As this liver-on-a-chip platform is a 3D culture system, it was thought that the diffusion between the three compartments (A1, A2, A3) could result in an overall decrease in the concentration which could be lessening the effect of CXCR4 antagonists. To overcome this, 40μM AMD3100 and AMD3465 were used in the A1 and invasion of MDA-MB-231 cells towards A2 was investigated for 72 hours (Figure 4.17).

Similar to the previous experiment, MDA-MB-231 invasion was observed in all the samples and showed a similar pattern with the first drug trial with 20μM AMD3100 and AMD3465 (Figure 4.15). AMD3465 added groups showed the highest migration towards A2 on Day 3. In the case of AMD3100 groups, it showed a similar pattern to drug-free groups. However, when all of the samples were compared with each other there were no significant differences in the migration distances again.

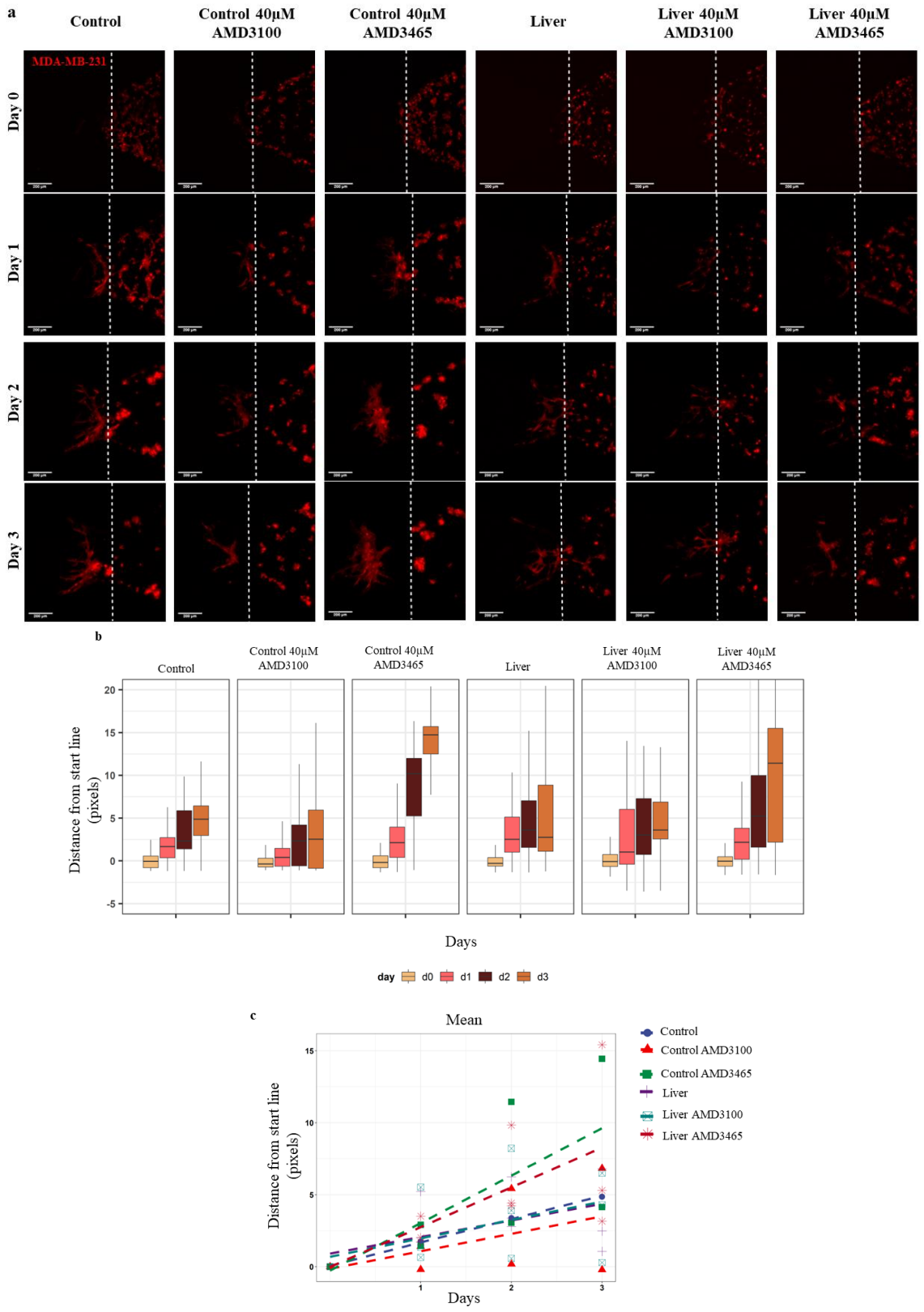

Figure 4.17. Invasion of MDA-MB-231 cells towards control versus liver in 40µM AMD3100 / AMD3465 presence and absence. Representative Z-stack images of MDA-MB-231 cells (red) invasion towards a) empty or liver-

embedded Matrigel (dashed line corresponds to the starting line for invasion) with the effect of CXCR4 antagonists (AMD3100 and AMD3465) (Scale bar: 200μm). b) Each bright pixel's distance to the starting line was calculated after thresholding of Z-stack images. The data normalized to Day 0 were plotted. c) Mean values of normalized distance distributions were plotted for Day 0 to Day 3. Liver pieces were obtained from the same mouse. All samples were not significant (not shown in the graph). (n=2, 3).

The fourth and final drug experiment was done with a similar logic to the third one which was eliminating the diffusion effect in our 3D model. In this case, rather than doubling the concentration of the CXCR4 antagonists in the A1 compartment, 20μM AMD3100 or AMD3465 were used in all the compartments (A1, A2, A3).

Matrigel was prepared with drug-free, 20μM AMD3100 or AMD3465 added Media C and after polymerization, MDA-MB-231 cells were prepared in Media C with 20μM AMD3100 or AMD3465 or no drug. For all the drug-free groups, Media F was loaded into the A3 compartments and for drug assays, Media F with 20μM AMD3100 or AMD3465 was used. So that the drug concentration would not be affected by the diffusion between the three compartments.

Figure 4.18 shows the overall data for this setup. It was seen that AMD3100 and AMD3465 did not inhibit the invasiveness of MDA-MB-231 cells toward A2 in this experiment as well and all the samples showed a similar migration pattern (Figure 4.18c). There was no significant difference between the groups except for control vs. liver. Similar to the first invasion assay experiment (Figure 4.14), liver presence showed a significantly increasing effect on MDA-MB-231 invasion ability.

When the outcome of this drug experiment and the previous two experiments were compared as a whole, it was determined that the problem of ineffective CXCR4 antagonists on invasion assay was not caused by diffusion or the liver-on-a-chip system. On the other hand, there are several possibilities such as AMDs may not inhibit CXCR4 as expected. The activity at the molecular levels of the antagonists was not assessed, which could be done for a better understanding of this behaviour. Also, concentrations might not be high enough or CXCR4 inhibition might be compensated by other factors in the liver environment. Lastly, CXCR4 may not be the main driver of MDA-MB-231 invasion towards the liver in this study. Hence CXCR4/CXCL12 axis was not disrupted,

and there were no significant changes in invasion in the presence of these drugs. To have a better understanding, other possible drivers could be targeted to perform drug assay.

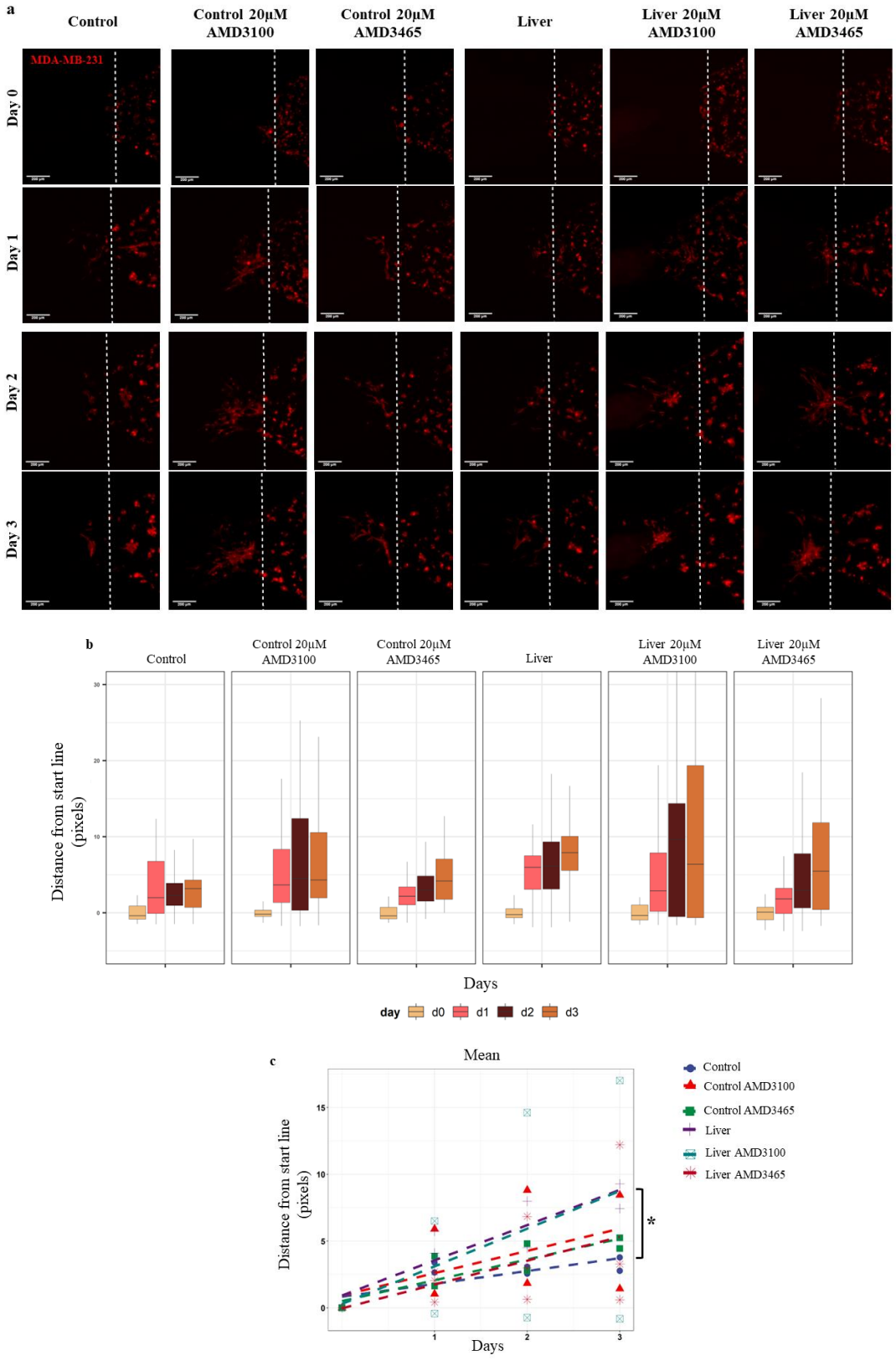

Figure 4.18. Invasion of MDA-MB-231 cells in the presence and absence of 20μM AMD3100 / AMD3465 in all three compartments of LOCs. Representative Z-stack images of MDA-MB-231 cells (red) invasion towards a) empty or liver-embedded Matrigel (dashed line corresponds to the starting line for invasion) with the effect of CXCR4 antagonists (AMD3100 and AMD3465) (Scale bar: 200μm). b) Each bright pixel's distance to the starting line was calculated after thresholding of Z-stack images. The data normalized to Day 0 were plotted. c) Mean values of normalized distance distributions were plotted for Day 0 to Day 2. Liver pieces were obtained from the same mouse. Non-significant data are not shown in the graph. (n=2, 3).

At the end of the invasion assays, it was seen that the location of the liver pieces was playing a role in the MDA-MB-231 invasion as well. Some samples had liver pieces closer to the invasion start line (dashed white lines in the invasion figures) while some pieces were located further away from the start line. MDA-MB-231 cell invasion distance from the start line was more in the samples with tissue nearby. This variable could be excluded by upgrading the liver-organ-on-a-chip platforms by changing the size or shape of the A2 of LOCs to ensure that each tissue is positioned the same distance from the start line. This would improve the accuracy of invasion analysis and would prevent the possibility of false assumptions.

CHAPTER 5

CONCLUSION

In recent years, a variety of studies had demonstrated the 3D modelling of the liver organ with different techniques such as liver-on-a-chip systems and PCLS cultures. Liver-on-a-chip systems are cell-based platforms that mimic the cellular architecture of the liver with the help of an ECM-mimicking scaffold gel such as collagen, alginate, gelatine, Matrigel or decellularized tissue matrix. However, as the liver organ has a complex structure with different types of cells, these systems fail to mimic the accurate physiology of the liver. Meanwhile in the case of PCLS, although it used the whole liver to obtain sections, it is a labour-intensive and sophisticated method that requires the usage of a vibratome and a suitable gel during the sectioning to prevent the disruption of the tissue. In light of this information, it was aimed to develop an accurate 3D model of the liver environment that needed less advanced equipment with a simple method.

In this study, different tissue processing methods were applied to the whole liver to obtain the most utilizable system. Both enzymatic and mechanic processes were compared for piece size, tissue integrity and texture, and application simplicity. Process IX, which was the usage of a needle gauge, was determined as the most labour-saving and simple method. This method was cost-effective as there were no specific high-cost equipment requirements and even so, there were no problems in obtaining reproducible homogenous samples within the desired range to support viability and functionality. Another advantage was that there were no enzymatic steps, which played a big role in reducing the cost as well.

To ensure the physiological state of the liver after the mechanical process viability and functionality assessments were done by using alamarBlue and albumin assays, respectively. Obtained data from these assays showed that alamarBlue incubation for tissue should be done for 20 hours to get the most accurate result possible. Also, the fluorescent intensity detection method for alamarBlue was seen to be more accurate than the colorimetric measurement for this study. Moreover, liver viability was significantly better when Media F containing 10 μg/mL insulin, 20 ng/mL EGF, 100 ng/mL cholera toxin, 0.5 μg/mL hydrocortisone, 1% Pen/Strep and 5% DHS in DMEM/F12 was used for both maintenance and culture steps. In addition to this, the

importance of 3 hours of incubation of obtained liver pieces at 37°C before Matrigel embedding was proved by alamarBlue results. Meanwhile, the albumin assay showed that there were no significant changes in the production of albumin between the first 48 hours with a slight decrease towards 72 hours which verified the preservation of liver function, and this finding was supported by the alamarBlue assay as well. In addition to these viability and functionality assays showed the importance of 3-hour incubation as well as media change in approximately every 24 hours to maintain the liver physiology.

In parallel with these experiments, scaffold gel optimization was done and Matrigel was chosen as the suitable ECM mimic for liver tissues compared to Collagen type I. During Collagen type I experiments, disruption in the gel border was observed which could be the result of enzymes in the liver tissue. When these findings were combined a 3D mimic model for the liver microenvironment named liver-organ-on-a-chip was established.

After the successful establishment of liver-organ-on-a-chip, invasion assay trials were done by using TNBC human breast carcinoma cell line, MDA-MB-231. It was observed that during the 72 hours of invasion investigation, MDA-MB-231 cells significantly migrated toward A2 of LOCs in the presence of liver more, compared to Matrigel-only control samples. As the next step, the effect of CXCR4 antagonists, AMD3100 and AMD3465 were investigated on the liver-on-a-chip platform by using them with a final concentration of 20μM and 40μM in different setups. For 20μM drug trials, three different LOC sets up were done to observe if there was a diffusion effect on the drug efficiency. However, all trials gave the same result in which there were no significant changes when the drug was present in the media. The inhibition of the CXCR4 pathway by AMD3100 and AMD3465 was not assessed thus it is possible that the inhibition was not successful. Also, there could be other chemoattractants in the liver environment that are masking the effect of CXCR4 antagonists on invasion. Hence, to understand the logistics behind the unsuccessful invasion inhibition, liver metabolism and enzyme activity can be checked in addition to the albumin production assessment to see if the drugs are metabolized by the liver organ.

Meanwhile, between the Matrigel-only samples, which were the control groups, and liver-embedded Matrigel groups there was a significant difference in the case of migrated distances of MDA-MB-231 cells in two experiment sets. However, for other sets, there was no significant difference which can be the result of a small sample size.

This could be improved by increasing the sample group size to get more accurate and precise statistical data.

As a future goal, these platforms can be further developed for other organs, cell lines and drugs, and can be used as a diagnostic kit for human tissue samples will help create better and more effective therapies.

REFERENCES

Brenner, C., Franz, W., Kühlenthal, S., Kuschnerus, K., Remm, F., Gross, L., … Kränkel, N. (2015). DPP-4 inhibition ameliorates atherosclerosis by priming monocytes into M2 macrophages. *International Journal of Cardiology*, *199*, 163-169. doi:10.1016/j.ijcard.2015.07.044

Cao, W., Chen, H., Yu, Y., Li, N., & Chen, W. (2021). Changing profiles of cancer burden worldwide and in China: A secondary analysis of the global cancer statistics 2020. *Chinese Medical Journal*, *134*(7), 783-791. doi:10.1097/cm9.0000000000001474

De Clercq, E. (2015). AMD3100/CXCR4 inhibitor. *Frontiers in Immunology*, *6*. doi:10.3389/fimmu.2015.00276

Ewart, L., Apostolou, A., Briggs, S. A., Carman, C. V., Chaff, J. T., Heng, A. R., … Levner, D. (2022). Performance assessment and economic analysis of a human liver chip for predictive toxicology. *Communications Medicine*, *2*(1). doi:10.1038/s43856-022-00209-1

Firatligil-Yildirir, B., Bati-Ayaz, G., Tahmaz, I., Bilgen, M., Pesen-Okvur, D., & Yalcin-Ozuysal, O. (2021). On-chip determination of tissue-specific metastatic potential of breast cancer cells. *Biotechnology and Bioengineering*, *118*(10), 3799-3810. doi:10.1002/bit.27855

Hatse, S., Princen, K., Clercq, E. D., Rosenkilde, M. M., Schwartz, T. W., Hernandez-Abad, P. E., … Schols, D. (2005). AMD3465, a monomacrocyclic CXCR4 antagonist and potent HIV entry inhibitor. *Biochemical Pharmacology*, *70*(5), 752-761. doi:10.1016/j.bcp.2005.05.035

Hughes, C. S., Postovit, L. M., & Lajoie, G. A. (2010). Matrigel: A complex protein mixture required for optimal growth of cell culture. *PROTEOMICS*, *10*(9), 1886-1890. doi:10.1002/pmic.200900758

Jia, Z., Cheng, Y., Jiang, X., Zhang, C., Wang, G., Xu, J., … Gao, Y. (2020). 3D culture system for liver tissue mimicking hepatic plates for improvement of human Hepatocyte (C3A) function and polarity. *BioMed Research International*, *2020*, 1-22. doi:10.1155/2020/6354183

Khan, S., Shin, J. H., Ferri, V., Cheng, N., Noel, J. E., Kuo, C., … Pratx, G. (2020). High-resolution positron emission microscopy of patient-derived tumour organoids. doi:10.1101/2020.07.28.220343

Koch, A., Saran, S., Tran, D. D., Klebba-Färber, S., Thiesler, H., Sewald, K., … Tamura, T. (2014). Murine precision-cut liver slices (PCLS): A new tool for studying tumour microenvironments and cell signaling ex vivo. *Cell Communication and Signaling*, *12*(1). doi:10.1186/s12964-014-0073-7

Kong, J., Luo, Y., Jin, D., An, F., Zhang, W., Liu, L., … Liu, T. (2016). A novel microfluidic model can mimic organ-specific metastasis of circulating tumor cells. *Oncotarget*, *7*(48), 78421-78432. doi:10.18632/oncotarget.9382

Ma, R., Feng, Y., Lin, S., Chen, J., Lin, H., Liang, X., … Cai, X. (2015). Mechanisms involved in breast cancer liver metastasis. *Journal of Translational Medicine*, *13*(1). doi:10.1186/s12967-015-0425-0

Makki, J. (2015). Diversity of breast carcinoma: Histological subtypes and clinical relevance. *Clinical Medicine Insights: Pathology*, *8*, CPath.S31563. doi:10.4137/cpath.s31563

Moradi, E., Jalili-Firoozinezhad, S., & Solati-Hashjin, M. (2020). Microfluidic organ-on-a-chip models of human liver tissue. *Acta Biomaterialia*, *116*, 67-83. doi:10.1016/j.actbio.2020.08.041

Murphy, P. M. (2001). Chemokines and the molecular basis of cancer metastasis. *New England Journal of Medicine*, *345*(11), 833-835. doi:10.1056/nejm200109133451113

O'Brien, J., Wilson, I., Orton, T., & Pognan, F. (2000). Investigation of the Alamar blue (resazurin) fluorescent dye for the assessment of mammalian cell cytotoxicity. *European Journal of Biochemistry*, *267*(17), 5421-5426. doi:10.1046/j.1432-1327.2000.01606.x

Rodriguez, A. D., Horowitz, L. F., Castro, K., Kenerson, H., Bhattacharjee, N., Gandhe, G., … Folch, A. (2020). A microfluidic platform for functional testing of cancer drugs on intact tumor slices. *Lab on a Chip*, *20*(9), 1658-1675. doi:10.1039/c9lc00811j

Schulze, R. J., Schott, M. B., Casey, C. A., Tuma, P. L., & McNiven, M. A. (2019). The cell biology of the hepatocyte: A membrane trafficking machine. *Journal of Cell Biology*, *218*(7), 2096-2112. doi:10.1083/jcb.201903090

Shi, Y., Riese, D. J., & Shen, J. (2020). The role of the cxcl12/Cxcr4/Cxcr7 Chemokine Axis in cancer. *Frontiers in Pharmacology*, *11*. doi:10.3389/fphar.2020.574667

Si-Tayeb, K., Noto, F. K., Nagaoka, M., Li, J., Battle, M. A., Duris, C., … Duncan, S. A. (2009). Highly efficient generation of human hepatocyte-like cells from induced pluripotent stem cells. *Hepatology*, *51*(1), 297-305. doi:10.1002/hep.23354

Spada, A., Emami, J., Tuszynski, J. A., & Lavasanifar, A. (2021). The uniqueness of albumin as a carrier in Nanodrug delivery. *Molecular Pharmaceutics*, *18*(5), 1862-1894. doi:10.1021/acs.molpharmaceut.1c00046

Spennati, G., Horowitz, L. F., McGarry, D. J., Rudzka, D. A., Armstrong, G., Olson, M. F., … Yin, H. (2021). Organotypic platform for studying cancer cell metastasis. *Experimental Cell Research*, *401*(2), 112527. doi:10.1016/j.yexcr.2021.112527

Sulava, E., Bergin, S., Long, B., & Koyfman, A. (2017). Elevated liver enzymes: Emergency department–focused management. *The Journal of Emergency Medicine*, *52*(5), 654-667. doi:10.1016/j.jemermed.2016.10.016

Sung, H., Ferlay, J., Siegel, R. L., Laversanne, M., Soerjomataram, I., Jemal, A., & Bray, F. (2021). Global cancer statistics 2020: Globocan estimates of incidence and mortality worldwide for 36 cancers in 185 countries. *CA: A Cancer Journal for Clinicians*, *71*(3), 209-249. doi:10.3322/caac.21660

Tian, H., Pang, J., Qin, K., Yuan, W., Kong, J., Ma, H., … Liu, T. (2019). A novel tissue-based liver–kidney-on-a-Chip can mimic liver tropism of Extracellular vesicles derived from breast cancer cells. *Biotechnology Journal*, *15*(2), 1900107. doi:10.1002/biot.201900107

Trefts, E., Gannon, M., & Wasserman, D. H. (2017). The liver. *Current Biology*, *27*(21), R1147-R1151. doi:10.1016/j.cub.2017.09.019

Valastyan, S., & Weinberg, R. (2011). Tumor metastasis: Molecular insights and evolving paradigms. *Cell*, *147*(2), 275-292. doi:10.1016/j.cell.2011.09.024

Wernberg, C. W., Ravnskjaer, K., Lauridsen, M. M., & Thiele, M. (2021). The role of diagnostic biomarkers, omics strategies, and single-cell sequencing for nonalcoholic fatty liver disease in severely obese patients. *Journal of Clinical Medicine*, *10*(5), 930. doi:10.3390/jcm10050930

Wheeler, S. E., Clark, A. M., Taylor, D. P., Young, C. L., Pillai, V. C., Stolz, D. B., … Wells, A. (2014). Spontaneous dormancy of metastatic breast cancer cells in an

all human liver microphysiologic system. *British Journal of Cancer*, *111*(12), 2342-2350. doi:10.1038/bjc.2014.533

Xing, F., Liu, Y., Huang, S., Lyu, X., Su, S. M., Chan, U. I., … Deng, C. (2021). Accelerating precision anti-cancer therapy by time-lapse and label-free 3D tumor Slice culture platform. *Theranostics*, *11*(19), 9415-9430. doi:10.7150/thno.59533

Yang, W., Wang, X., & Wang, Z. (2022). Engineered liver tissue *in vitro* to mimic liver functions and its biomedical applications. *Materials Advances*, *3*(10), 4132-4154. doi:10.1039/d2ma00144f

Yao, Q., Xu, C., Zhao, H., & Chen, H. (2015). CXCR4 in breast cancer: Oncogenic role and therapeutic targeting. *Drug Design, Development and Therapy*, 4953. doi:10.2147/dddt.s84932

Ye, S., Boeter, J. W., Penning, L. C., Spee, B., & Schneeberger, K. (2019). Hydrogels for liver tissue engineering. *Bioengineering*, *6*(3), 59. doi:10.3390/bioengineering6030059

Yeeravalli, R., & Das, A. (2021). Molecular mediators of breast cancer metastasis. *Hematology/Oncology and Stem Cell Therapy*, *14*(4), 275-289. doi:10.1016/j.hemonc.2021.02.002

Ziyao, L., Jingzhe, W., & Huabiao, C. (2021). CXCR4 antagonist AMD3100 (Plerixafor) modulates immune responses in the tumor microenvironment. *International Journal of Cancer and Clinical Research*, *8*(1). doi:10.23937/2378-3419/1410144